

<https://helda.helsinki.fi>

The blood vasculature instructs lymphatic patterning in a SOX7-dependent manner

Chiang, Ivy K. N.

2023-03

Chiang , I K N , Graus , M S , Kirschnick , N , Davidson , T , Luu , W , Harwood , R , Jiang , K , Li , B , Wong , Y Y , Moustaqil , M , Lesieur , E , Skoczylas , R , Kouskoff , V , Kazenwadel , J , Arriola-Martinez , L , Sierrecki , E , Gambin , Y , Alitalo , K , Kiefer , F , Harvey , N L & Francois , M 2023 , ' The blood vasculature instructs lymphatic patterning in a SOX7-dependent manner ' , EMBO Journal , vol. 42 , no. 5 , e109032 . <https://doi.org/10.15252/emj.2021109032>

<http://hdl.handle.net/10138/355484>

<https://doi.org/10.15252/emj.2021109032>

cc_by_nc_nd

publishedVersion




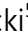


Downloaded from Helda, University of Helsinki institutional repository.

This is an electronic reprint of the original article.

This reprint may differ from the original in pagination and typographic detail.

Please cite the original version.

The blood vasculature instructs lymphatic patterning in a SOX7-dependent manner

Ivy K N Chiang¹, Matthew S Graus¹, Nils Kirschnick², Tara Davidson¹, Winnie Luu¹, Richard Harwood³, Keyi Jiang¹, Bitong Li¹ , Yew Yan Wong⁴ , Mehdi Moustaqil⁵, Emmanuelle Lesieur⁶, Renae Skoczylas⁶, Valerie Kouskoff⁷, Jan Kazenwadel⁸ , Luis Arriola-Martinez⁸, Emma Sierecki⁵ , Yann Gambin⁵, Kari Alitalo⁹ , Friedmann Kiefer², Natasha L Harvey⁸ & Mathias Francois^{1,4,*} 

Abstract

Despite a growing catalog of secreted factors critical for lymphatic network assembly, little is known about the mechanisms that modulate the expression level of these molecular cues in blood vascular endothelial cells (BECs). Here, we show that a BEC-specific transcription factor, SOX7, plays a crucial role in a non-cell-autonomous manner by modulating the transcription of angiocrine signals to pattern lymphatic vessels. While SOX7 is not expressed in lymphatic endothelial cells (LECs), the conditional loss of SOX7 function in mouse embryos causes a dysmorphic dermal lymphatic phenotype. We identify novel distant regulatory regions in mice and humans that contribute to directly repressing the transcription of a major lymphangiogenic growth factor (*Vegfc*) in a SOX7-dependent manner. Further, we show that SOX7 directly binds HEY1, a canonical repressor of the Notch pathway, suggesting that transcriptional repression may also be modulated by the recruitment of this protein partner at *Vegfc* genomic regulatory regions. Our work unveils a role for SOX7 in modulating downstream signaling events crucial for lymphatic patterning, at least in part via the transcriptional repression of VEGFC levels in the blood vascular endothelium.

Keywords blood vessels; gene regulation; lymphatic endothelial cell; SOX transcription factor; VEGFC

Subject Categories Development; Vascular Biology & Angiogenesis

DOI 10.15252/embj.2021109032 | Received 22 June 2021 | Revised 15 December 2022 | Accepted 22 December 2022 | Published online 30 January 2023

The EMBO Journal (2023) 42: e109032

Introduction

The long-standing observation of parallel networks between arteries and lymphatic vessels has hinted at a role for the blood vessels in guiding lymphatic patterning during embryogenesis (Kampmeier, 1969). This influence of the blood vasculature on the trajectory of lymphatic vessels has been shown using both zebrafish and mouse model systems (Bussmann *et al*, 2010; Vaahtomeri *et al*, 2017). It has been established that blood endothelial cells (BECs) produce lymphangiogenic guidance cues such as chemokine receptor 4/chemokine ligand 12, adrenomedullin, and semaphorin3G (Cha *et al*, 2012; Uchida *et al*, 2015; Liu *et al*, 2016). In addition to the blood vasculature, other tissues such as the mesenchyme and immune cells play a critical role in informing lymphatic vessel assembly (Karkkainen *et al*, 2004; Gordon *et al*, 2010; Cahill *et al*, 2021), mostly via the production of vascular endothelial growth factor-C (VEGFC) (Rauniyar *et al*, 2018). During the early steps of lymphangiogenesis, VEGFC from the mesenchyme stimulates the exit of specified lymphatic endothelial cell (LEC) progenitors from the cardinal veins (CVs) and intersomitic veins, and a subsequent dorso-lateral migration to form the lymphatic plexus (Karkkainen *et al*, 2004). Loss of VEGFC function results in the failure of LECs to form a primary vascular network, and a disorganized accumulation of LEC progenitors within the walls of the CVs.

Despite a plethora of information on the mode of action, maturation process, and signaling mechanisms of VEGFC, there is a lack of understanding of how this growth factor is transcriptionally regulated, especially in the endothelial compartment. While the hematopoietically expressed homeobox (HHEX) genetic pathway has been implicated as an endothelial-specific regulator upstream of VEGFC expression, only the BTB and CNC homology (BACH) family

1 The Centenary Institute, David Richmond Program for Cardio-Vascular Research: Gene Regulation and Editing, Sydney Medical School, University of Sydney, Sydney, NSW, Australia

2 European Institute for Molecular Imaging (EIMI), University of Münster, Münster, Germany

3 Sydney Microscopy and Microanalysis, University of Sydney, Sydney, NSW, Australia

4 The Genome Imaging Center, The Centenary Institute, Sydney, NSW, Australia

5 EMBL Australia Node in Single Molecule Science, and School of Medical Sciences, University of New South Wales, Sydney, NSW, Australia

6 Institute for Molecular Bioscience, The University of Queensland, St. Lucia, QLD, Australia

7 Division of Developmental Biology & Medicine, The University of Manchester, Manchester, UK

8 Centre for Cancer Biology, University of South Australia and SA Pathology, Adelaide, SA, Australia

9 Wihuri Research Institute and Translational Cancer Medicine Program, Faculty of Medicine, University of Helsinki, Helsinki, Finland

*Corresponding author. Tel: +61 28627 9497; Fax: +61 28627 4716; E-mail: m.francois@centenary.org.au

of transcription factors have been shown to directly transactivate the VEGFC promoter and these experiments were performed in human ovarian carcinoma ES2 cells (Schuermann *et al.*, 2015; Gauvrit *et al.*, 2018; Cohen *et al.*, 2020). Thus, there is still a paucity of information on the molecular mechanisms that drive *Vegfc* transcription in the endothelial cell context, despite the fact that it is well-established that endothelial-derived VEGFC is critical for blood vessel angiogenesis and coronary artery formation (Cao *et al.*, 1998; Chen *et al.*, 2014).

The SOX group F (SOXF) transcription factors (SOX7, SOX17, and SOX18) are known to play a conserved role in vascular development (François *et al.*, 2010; Yao *et al.*, 2019). It has been reported that SOXF factors interact genetically with both VEGFR2 and VEGFD to create a positive feedback loop during blood vascular angiogenesis (Duong *et al.*, 2013; Kim *et al.*, 2016). In these studies, VEGF was shown to enhance SOX7 and SOX17 expression, and modulate the nuclear localization of the SOXF proteins. SOX7 and SOX17, in turn, upregulate the expression of VEGF receptor, VEGFR2. In addition, SOXF proteins function directly upstream of the Notch pathway by modulating the activities of the *Dll4* and *Notch1* enhancers (Saciotto *et al.*, 2013; Chiang *et al.*, 2017). Taken together, these lines of evidence established a major regulatory axis between SOXF, VEGFs, and the Notch pathway, most likely at play during both arteriovenous specification and angiogenesis. However, it remains elusive whether this signaling axis is also involved in other vascular remodeling processes.

Here, we show that SOX7 plays a pivotal role in controlling lymphatic vessel morphogenesis, at least in part via a repressive mechanism of *Vegfc* transcription in the blood endothelium. Endothelial-specific loss of SOX7 function during the early steps of lymphatic specification in mouse embryos results in both an ectopic distribution of PROX1-positive LEC progenitors in the medio-ventral aspects of the CVs, and disruption of organ-specific lymphatic vessel morphogenesis. In particular, this is characterized by an excessive emergence of endomucin (EMCN) derived LEC progenitors in the dermal vasculature. Consistent with a role for SOX7 in the transcriptional repression of *Vegfc*, we demonstrated an upregulation of BEC-derived *Vegfc* upon depletion of SOX7 in both *in vivo* and *in vitro* model systems. Genome-wide analysis of SOX7-binding locations *in vivo* revealed that this transcription factor directly binds to putative repressive distal regulatory regions upstream of VEGFC transcription start sites, in both human and mouse. Finally, we showed that SOX7 physically interacts with the Notch effector and transcriptional repressor, HEY1, suggesting indirect transcriptional repression of *Vegfc* mediated by Notch signaling. This study identifies SOX7 as the first direct endothelial-specific regulator of *Vegfc* transcription and uncovers novel mechanisms that likely underlie the SOX7-mediated fine-tuning of VEGFC expression in BECs, a process essential for correct lymphatic growth and patterning.

Results

The SOX7 BEC-specific transcription factor is necessary for dermal lymphatic patterning

While it is known that blood vessels instruct the patterning of lymphatic vessels in a paracrine manner, little is known about how

the expression levels of guiding molecules from blood vessels are transcriptionally regulated. To address this, we took advantage of the loss-of-function of the mouse SOX7 transcription factor, which expresses specifically in blood endothelial cells (BECs) but not in lymphatic endothelial cells (LECs) (Kim *et al.*, 2016). The endogenous expression profile of SOX7 was determined using a *Sox7*-V5 tagged transgenic reporter mouse line (Appendix Fig S1). Briefly, the V5 epitope was knocked in within the C-terminal domain of *Sox7* to specifically label endogenous SOX7 expression. *Sox7*-V5 homozygous animals are fertile and viable. The *Sox7*-V5 tagged protein was detected specifically in endothelial cell (EC) nuclei of both the cardinal veins (CVs) and the dorsal aortae (DA) (Appendix Fig S2A), consistent with a previous report (Kim *et al.*, 2016). While SOX7 was detected in some ECs of the CVs (Appendix Fig S2A), none was observed in mature veins and venules in embryonic skin (Appendix Fig S2B). High levels of *Sox7*-V5 were observed in arterioles near the midline but only low levels of SOX7 were detected in mature SOX7-positive arteries (Appendix Fig S2B). These observations were further supported by immunofluorescence analysis for β -galactosidase (β -gal) in E14.5 embryonic skin of a *Sox7 lacZ* knock-in mouse line (Appendix Fig S2C–F). Further assessment of SOX7 endogenous expression level in LEC revealed that this TF is not co-expressed in PROX1-positive cells during skin organogenesis (Fig EV1A) and as previously reported (Kim *et al.*, 2016). By contrast, the SOX7 TF is often observed in BECs that are closely associated with the developing lymphatics (Fig EV1A). Expression profiling during the early step of lymphangiogenesis (E11.5) in the cardinal vein showed that this TF is expressed in a subset of PROX1-positive LEC progenitors (34%) and that this expression is reduced to 7% when LECs have exited the vessel wall and migrate in the mesenchyme (Fig EV1B–D). This approach also revealed certain heterogeneity in the venous endothelial cell population, which displays PROX1^{high}/SOX7^{low} and PROX1^{low}/SOX7^{high} profiles (Fig EV1C white arrowheads and asterisks, respectively).

To explore the role of SOX7 in lymphatic vascular remodeling, we took advantage of a SOX7 loss-of-function mouse model. It has been shown that *Sox7*^{-/-} homozygous mutants die *in utero* by E10.5 (Kim *et al.*, 2016; Lilly *et al.*, 2017), so we used an endothelial-specific Cre-inducible mouse line, the *Cdh5-CreERT2:Sox7 fl/fl* mouse line. Tamoxifen-induced excision of *Sox7* exon 2 was performed at E9.5 and E10.5, the stage of early LEC specification in the CVs (Wigle & Oliver, 1999; Srinivasan *et al.*, 2007). Cre efficiency was initially validated by a single pulse of tamoxifen at E9.5, followed by analysis at E10.5 (Fig 1A). Further analysis followed tamoxifen doses at E9.5 and E10.5. At E14.5, the Cre-inducible endothelial-specific *Sox7* knockout (*Sox7*^{iECKO}) mutant embryos appeared similar in size to their sibling controls but displayed gross subcutaneous edema, with some showing blood-filled lymphatic vessels (Fig 1B, Appendix Fig S3, 80% of mutant with edema out of $n = 5$). While gross edema is less obvious a day earlier at E13.5 (Fig 1C), detailed analysis of dermal lymphatics revealed that lymphatic vessels in the *Sox7*^{iECKO} mutants were severely dilated, lacked intervessel branches and showed migration defects (Fig 1C–F). Although there is a decrease in total PROX1⁺ cells in the skin from the flank (Fig 1G), quantitative analysis of PROX1⁺ nuclei normalized to LEC branches across the entire skin sample (flank + midline) showed a significant increase in the mutant (Fig 1H and I),

suggesting LEC hyperproliferation coupled to a failure of vessel remodeling. Lymphatic defects were also observed in other organs such as the developing gut, whereby an aberrant and mis-patterned network showed excessive remodeling of NRP2 positive vessels (Appendix Fig S4). Relative to sibling controls, most LECs in the *Sox7^{iECKO}* mutant embryos assemble in islands or clusters that appeared disconnected from the main network (Fig 1C, J). Consistent with the gross edema observed at E14.5, the dermal lymphatic phenotype persists, and appeared further aggravated at this stage (Fig EV2A). Unlike the lymphatic vessels, blood vessel morphogenesis is less severely affected in E13.5 *Sox7^{iECKO}* mutant embryos (Fig 1C). Apart from increased blood vessel density at the angiogenic front, which is accompanied by an increase in the proportion of proliferative ERG⁺ endothelial cells (Fig EV2B); overall the blood vessel network in *Sox7^{iECKO}* mutant embryos appeared intact and comparable to sibling controls.

To rule out the possibility that the observed lymphatic patterning defect is due to *CreERT2* toxicity (Brash et al, 2020), we created *Cdh5-CreERT2: Sox7 fl/fl*; mT/mG and *Cdh5-CreERT2: mT/mG* animals. The mT/mG double fluorescence Cre-reporter mice express the tdTomato red fluorescent protein prior to Cre-mediated excision, and green fluorescent protein after excision, therefore allowing *Cdh5-CreERT2* activity to be measured and traced (Muzumdar et al, 2007). To effectively quantify *Cdh5-CreERT2* activity, mice were pulsed with tamoxifen at E12.5, and embryos were harvested at E14.5 (Fig EV2C). Despite showing comparable *CreERT2* activity to sibling controls (Fig EV2D and E), *Sox7^{iECKO}; mT/mG* embryos consistently showed dilated lymphatic vessels with reduced branching points (Fig EV2F and G) but no obvious blood vascular defects (Fig EV2H). This suggests that the mis-patterning of dermal lymphatics observed in *Cdh5-CreERT2: Sox7 fl/fl* embryo is dependent on SOX7 loss-of-function. Furthermore, in order to exclude a possible contribution of dermal lymphatic defects secondary to an early interference with the early stage of LEC specification in the vein, we induced *Sox7* gene deletion at E11.5 and E12.5. Genetic disruption of *Sox7* function in that time window also recapitulated the phenotype observed with an earlier schedule of tamoxifen treatment (e.g., defloxing at E9.5 and E10.5, Fig EV2I). As a final demonstration that *Sox7* loss-of-function is a driver of a lymphatic-specific phenotype, we analyzed the morphogenesis of the initial lymphatic vascular plexus in *Sox7^{iECKO}* at E11.5 after defloxing at E9.5 and E10.5. This reduced time window approach of *Sox7* deletion showed that LEC specification in the CV is not affected (Fig EV2J, white arrowheads) and the lymph sacs do form but appear nonfunctional since these structures are filled with red blood cells (Fig EV2K, white arrows).

Lastly, SOX7 and PROX1 co-expression in the cardinal vein at the early time point of LEC specification raised the possibility that the lymphatic vascular phenotype associated with *Sox7* loss-of-function might arise in a cell-autonomous manner. To assess this potential mechanism, we deleted specifically the *Sox7* gene in the LEC progenitors by taking advantage of a *Prox1-CreERT2* driver. The *Sox7* genetic disruption during the onset of lymphatic endothelial cell specification in the cardinal vein (E9.5 and E10.5) did not yield any phenotype (Fig EV3). Together, these results show that tightly regulated BEC-specific SOX7 expression is essential for proper patterning of the lymphatic network, likely via the modulation of angiocrine factors.

SOX7 is a negative regulator of VEGFC transcription in blood vascular endothelial cells

The expression profile of SOX7 in angiogenic blood vessels (Appendix Fig S2B) (del Toro et al, 2010), combined with the observation of lymphatic patterning defects in SOX7 loss-of-function mouse embryos, prompted us to investigate the levels of lymphangiogenic molecules in BECs. To profile angiocrine signals in BEC during development, we performed single-nuclei RNA-Seq on whole skin from wild-type mouse embryos at E14.5. This approach reveals that only BECs and a sub-population of neurons and smooth muscle cells actively transcribe *Vegfc* during dermal embryogenesis (Fig EV4). Consistent with the immunofluorescence analysis in Fig EV1A, we observed *Sox7* expression in skin is restricted to endomucin-positive BECs with no expression in *Prox1*-positive LECs or other nonendothelial cell types at E14.5 (Figs 2A and EV4A–D). Interestingly, no *Vegfc* transcripts were detected in *Prox1*-positive LECs (Figs 2B and EV4B); suggesting therefore VEGFC autocrine signaling is not at play in dermal LECs. Co-expression of *Sox7* and *Vegfc* transcripts in a subset of endomucin-positive BECs raises the possibility that SOX7 may transcriptionally regulate *Vegfc* in a fraction of the endothelium compartment (Fig 2A and B, red arrowheads). We then sorted BECs and LECs from E14.5, E16.5, and E18.5 mouse embryonic skins (Kazenwadel et al, 2012) and performed microarray analysis on both cell populations. This approach confirmed that during development, BECs express *Vegfc* mRNA at 1.5- to 2.9-fold higher levels than LECs (Fig EV4E). Since the SOX7 TF has a wide range of direct target genes (like *Notch1*, *Dll4*, and *Vegfr2*) that are also important for vessel morphogenesis (Sacilotto et al, 2013; Kim et al, 2016; Chiang et al, 2017), the mechanism behind the lymphatic phenotype reported in Fig 1 is likely to involve *Vegfc* transcriptional interference in combination with disruption of multiple pathways. We assessed *Sema3e* and *Plxnd1*, both known to be at play to regulate LEC and BEC interaction (Liu et al, 2016; Maruyama et al, 2021). We then assessed the expression of both molecules in BEC and could only detect *Plxnd1* (Fig EV4F). Measuring the expression levels of *Plxnd1* in BECs, comparing control and *Sox7^{iECKO}*, did not reveal any significant changes for this gene (Fig EV4G). This suggests that other guidance molecules, but neither *Plxnd1* nor *Sema3e*, are at play and prompted us to explore further the role of *Vegfc*.

High levels of *Vegfc* transcripts in BECs were further validated in mouse wild-type embryos using *Vegfc* single-molecule RNA fluorescent *in situ* hybridization (smFISH) analysis at around E11.5 (Fig 2C). Thick serial sections of wild-type embryos were labeled for *Vegfc* (pink), PECAM (white) and *Gapdh* (green), demonstrating that BEC-specific endogenous levels of *Vegfc* are enriched in the dorsal aorta compartment (Fig 2C, pink arrows, and Appendix Fig S5) and in the mesenchyme surrounding the dorso-lateral territories of the cardinal vein. This further validates VEGFC expression in BECs, which has been observed previously in developing mouse and zebrafish DA, by immunostaining and *in situ* hybridization assay, respectively (Karkkainen et al, 2004; Tammela et al, 2008; Hogan et al, 2009).

To assess whether the VEGF/VEGFR pathway is affected at a transcriptional level by loss of SOX7 function, we compared the expression of key genes by qPCR profiling of sorted CD31⁺CD45⁻ endothelial cells from the skin of E14.5 control and *Sox7^{iECKO}*

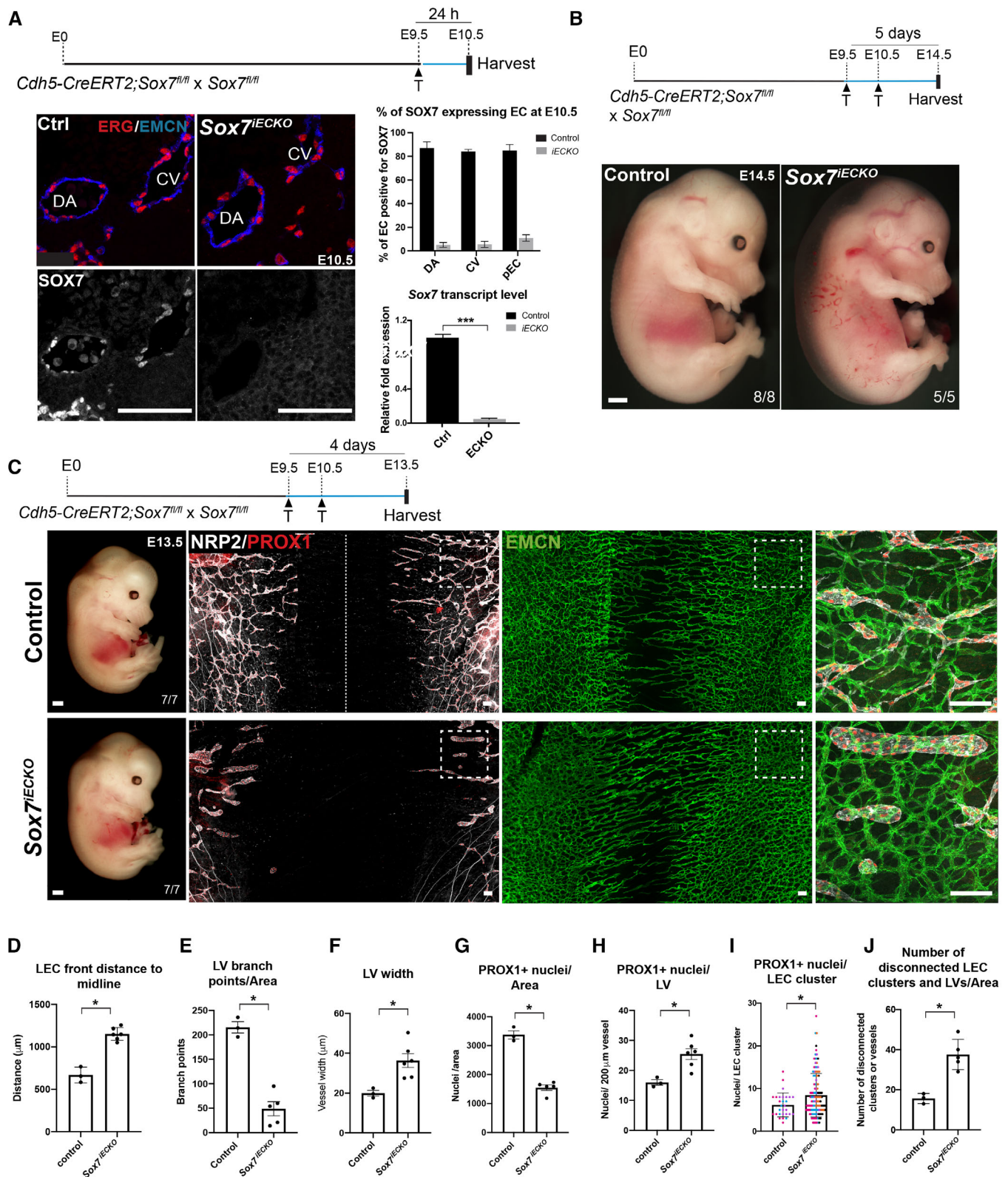


Figure 1. Conditional loss of Sox7 function in blood vascular endothelial cells causes dermal lymphatic patterning defects.

- A** Tamoxifen schedule: the pulse of the pregnant dam at E9.5, harvest at E10.5. Representative fluorescent immune staining of E10.5 *Sox7^{IECKO}* mutants and sibling control embryos. The endothelium is delineated by endomucin (EMCN) (blue) and endothelial cells by ETS-related gene (ERG) (red), SOX7-positive cells are shown in white. (Top right graph) The percentage of SOX7-positive endothelial cells in different vascular beds, quantified from 10 sequential transverse sections in 2 control and 3 *Sox7^{IECKO}* mutants. (Bottom right panel) Graph indicating the levels of *Sox7* transcript in sibling controls and *Sox7^{IECKO}* mutants. Mean \pm SEM; scored sibling control, $n = 9$; *Sox7^{IECKO}* mutants, $n = 7$; Mann–Whitney *U*-test. $P < 0.0005$ (***)
- B** Brightfield images of *Sox7^{IECKO}* mutants and sibling controls at E14.5, after tamoxifen-induced CRE activity at E9.5 and E10.5. Scored sibling controls, $n = 8$; *Sox7^{IECKO}* mutants, $n = 5$.
- C** Brightfield images and whole-mount immunostaining of *Sox7^{IECKO}* mutant and sibling control skin at E13.5, after Cre induction at E9.5 and E10.5. Dermal lymphatic structures are marked by neuropilin-2 (NRP2) (membranous white), lymphatic endothelial cells by Prospero-related homeobox 1 (PROX1) (red), and blood vessels by EMCN (green). Dash line represents the midline of the embryo. Scored sibling controls, $n = 7$; *Sox7^{IECKO}* mutants, $n = 7$.
- D–H** Quantification of (D) Distance of the lymphatic vessel front from the midline (μm) (E) lymphatic branch points/area (F) lymphatic vessel width (μm) (G) PROX1⁺ nuclei/area and (H) PROX1⁺ nuclei/lymphatic vessels across the whole skin. Total area = $4,200 \times 1,500 \mu\text{m}$ on both sides of the midline, in sibling controls ($n = 3$) and *Sox7^{IECKO}* mutants ($n = 5$ –6). (F, H) Average of width and PROX1⁺ nuclei was obtained from 7 random representative leading lymphatic vessels, of fixed length at $200 \mu\text{m}$, from both sides of the midline in each skin.
- I, J** Quantification of (I) PROX1⁺ nuclei in each LEC cluster with each color dot representing a different embryo and (J) disconnected lymphatic endothelial cell (LEC) clusters ($< 100 \mu\text{m}$) and vessel branches ($> 100 \mu\text{m}$)/area. Total area quantified = $4,200 \times 2,200 \mu\text{m}$ on both sides of midline in sibling controls ($n = 3$) and *Sox7^{IECKO}* mutants ($n = 5$). PROX1⁺ nuclei were quantified from $n = 29$ and $n = 122$ LEC clusters, respectively.

Data information: In (D–J), skins were dissected from the cervico-thoracic regions of E13.5 embryos and defloxed at E9.5 and E10.5. Mean \pm SEM, Mann–Whitney *U*-test. $P < 0.05$ (*). Statistical analysis using the number of embryos as a “ n ” number in (I), with sibling controls ($n = 3$) and *Sox7^{IECKO}* mutants ($n = 5$), reveals similar statistical significance as when LEC clusters are used as a “ n ” number. LV—lymphatic vessel. Scale bars = $100 \mu\text{m}$ (immunofluorescence images A, C), 1 mm (bright-field images B, C).

Source data are available online for this figure.

embryos, following tamoxifen induction at E11.5 and E12.5 (Figs 2D and EV2I). This analysis showed a significant upregulation of *Vegfc* mRNA levels in *Sox7^{IECKO}* mutant cells. To test whether SOX7 cell autonomously regulates *VEGFC* transcript levels in BECs, we next reduced levels of SOX7 using a siRNA-based approach in human EC lines (HUAECs and HUVECs). At 30 h post-siRNA transfection, we observed a two-fold increase in the level of *VEGFC* transcripts in HUAECs (Fig 2E). To reduce the number of potential secondary hits mediating the increase in *VEGFC* levels downstream of SOX7, gene expression analysis was performed at 17 h post-SOX7 gene depletion. Both HUAECs and HUVECs showed a significant increase in *VEGFC* transcript levels in response to depleted SOX7 function (Fig 2F and G). A significant reduction in *VEGFR2* transcripts was only observed in SOX7 siRNA-depleted HUVECs but not HUAECs, suggesting that transcriptional regulation of *VEGFR2* by SOX7 is context-dependent. The consistent upregulation of *VEGFC* in response to SOX7 gene depletion both *in vivo* and *in vitro* implies that *VEGFC* is an early response gene that is negatively regulated by SOX7 activity.

SOX7 represses VEGFC indirectly through upregulation of the Notch effector HEY1

Having established that BEC-specific expression of *VEGFC* is regulated by SOX7 activity, we next investigated how SOX7 might exert its repressive effects on *VEGFC* gene expression. The Notch signaling pathway has been previously shown to negatively regulate the specification of LECs in the ventro-medial aspects of the CVs, with ectopic Notch signaling reducing levels of the LEC specification regulator, PROX1 (Murtomaki et al, 2013). This finding, together with the known role of SOX7 in the regulation of *Notch1/Dll4* transcription (Sacilotto et al, 2013; Chiang et al, 2017), leads us to postulate that SOX7 may negatively regulate *Vegfc* through modulation of the Notch pathway. To evaluate the level of Notch activity in the context of SOX7 loss-of-function, we assessed the transcript levels of key Notch pathway members in sorted CD31⁺CD45[−]

endothelial cells from E14.5 mouse skin samples. We observed a significant downregulation of the Notch effector, *Hey1*, but not *Dll4* and *Notch1*, in cells from *Sox7^{IECKO}* embryos versus sibling controls (Fig 3A). In siRNA experiments in human cells, at 17 h post-siSOX7 transfection levels of both *DLL4* and *HEY1* were consistently reduced in HUAECs and HUVECs (Fig 3B and C).

HEY1 is a known transcriptional repressor that exerts its repressive activity through its basic helix-loop-helix (bHLH) domain (Nakagawa et al, 2000; Fischer et al, 2005). HEY1 has been shown to suppress the VEGFC receptor, VEGFR3 (Murtomaki et al, 2013). To test whether HEY1 could also directly repress VEGFC, we overexpressed HEY1 in HeLa cells transfected with a synthetic construct containing a luciferase reporter gene fused to either a mouse or a human VEGFC promoter fragment (Chilov et al, 1997; Huang et al, 2014). In both cases, we found that HEY1 over-expression significantly reduced the VEGFC promoter activity (Fig 3D), showing that HEY1 has the capacity to repress *Vegfc* transcription. Together, these observations support that SOX7 indirectly represses *Vegfc* through transactivation of the Notch effector and transcriptional repressor, HEY1.

SOX7 interacts with transcriptional repressor, HEY1

In addition to directly regulating gene transcription, there is a growing body of evidence suggesting that SOXF factors modulate gene expression through protein-protein interactions (PPIs) with other transcription factors (Hosking et al, 2001; Sacilotto et al, 2013; Lilly et al, 2016; Overman et al, 2017). Given that Sox7 and Hey have been previously shown to genetically interact in the zebrafish vasculature (Hermkens et al, 2015), we investigated whether SOX7 physically interacts with HEY1 directly through PPIs.

To screen for PPIs in a low-throughput manner, we used a cell-free protein production system (*Leishmania Tarentolae*) combined with an Amplified Luminescent Proximity Homogenous (ALPHA) Screen assay. This approach enabled us to assess multiple pairwise interactions between SOX7 and other SOXF members (e.g., SOX17

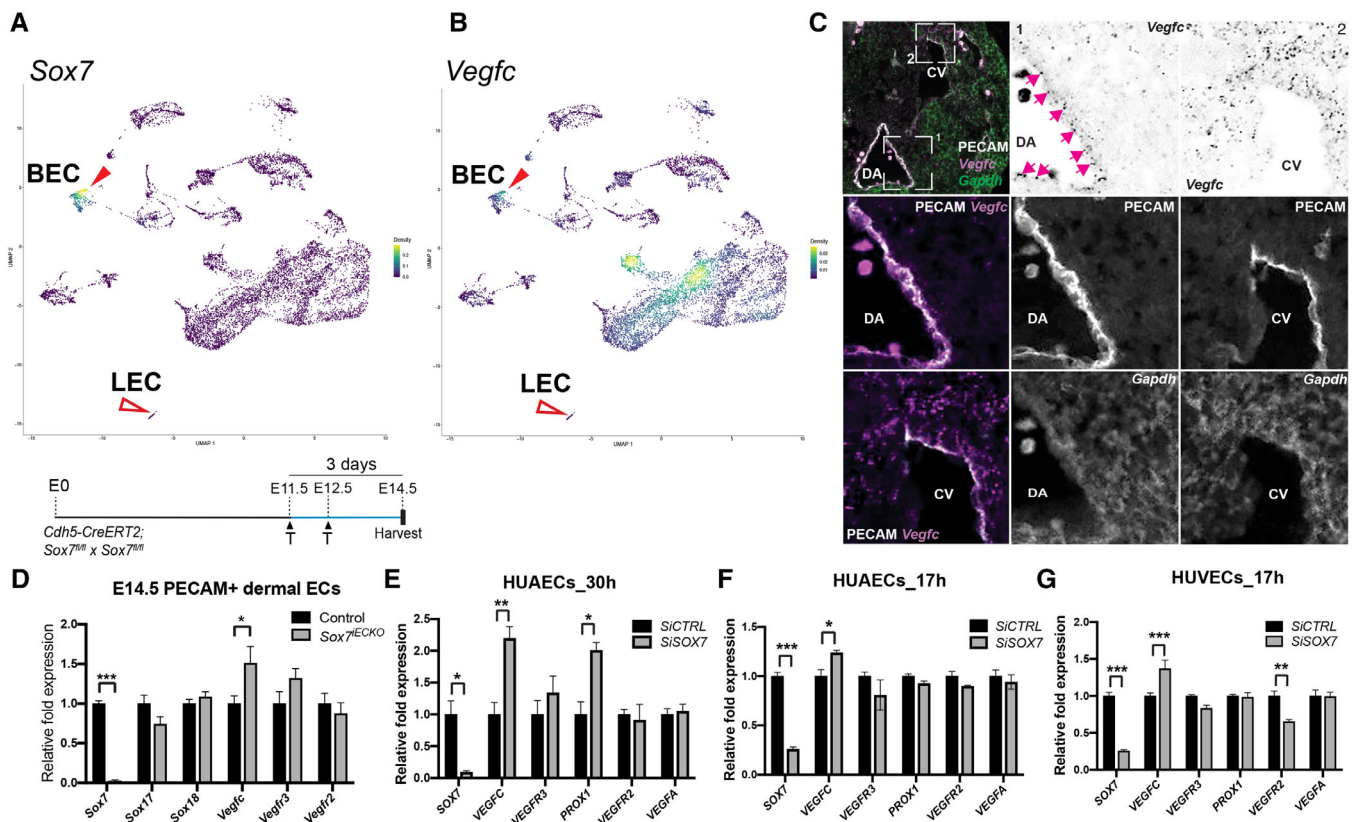


Figure 2. Loss of *Sox7* function upregulates *Vegfc* transcript levels in blood endothelial cells.

- A, B** Nebulosa plots from single-nuclei RNA-Seq on E14.5 embryonic skins, showing the expression of *Sox7* and *Vegfc*. Both *Sox7* and *Vegfc* are found expressed in BECs (red arrowheads) but not LECs (empty red arrowheads).
- C** Arterial endothelial cells express *Vegfc* transcripts. Transverse section of a E10.5 wild-type embryo stained by single-molecule FISH (smFISH) for *Gapdh* (green) and *Vegfc* (magenta) and immuno-stained for PECAM (white). The first panel shows a merged version of the pseudo-color signals for the 3 markers. Inset 1 shows the expression of *Vegfc* in the endothelial cell of the dorsal aorta (black and white, pink arrows). Inset 2 shows the high expression levels of mesenchymal *Vegfc* expressed in the dorso-lateral aspects of the cardinal vein.
- D** qPCR on FACS-sorted PECAM⁺CD45⁻ endothelial cells of *Sox7*^{IECKO} mutants and sibling controls at E14.5, after Cre induction at E11.5 and E12.5. Expression is normalized to endothelial markers *Pecam* and *Cdh5*. Scored sibling controls, $n = 9$; *Sox7*^{IECKO} mutants, $n = 8$.
- E, F** qPCR on human arterial endothelial cells (HUAECs) transfected with *SISOX7* or *SICTRL* for (E) 30 h and (F) 17 h.
- G** qPCR on human venous endothelial cells (HUVECS) transfected with *SISOX7* or *SICTRL* for 17 h.

Data information: In (E–G), expression is relative to *HPRT* and *GAPDH*. Data from one siRNA experiment performed in triplicates. (D–G) Mean \pm SEM; t-test. $P < 0.05$ (*); $P < 0.005$ (**); $P < 0.0005$ (***). BEC—blood endothelial cell; LEC—lymphatic endothelial cell; DA—dorsal aorta; CV—cardinal vein; Dors.—dorsal; Med.—medial. Scale bars = 100 μ m.

Source data are available online for this figure.

and SOX18), and key effectors of the Notch pathway such as RBPJ and HEY1, as well as other transcription factors such as GATA2. We used well-characterized PPIs such as SOX18/SOX18 homodimer and SOX18/RBPJ, or SOX18/MEF2C heterodimer (Overman *et al*, 2017; Moustaqil *et al*, 2018), as positive controls to calibrate the strength of the ALPHAScreen signal. An ALPHAScreen signal of medium and high coincidence was detected for SOX7/RBPJ and SOX7/HEY1, respectively, suggesting robust direct PPIs (Fig 3E). To further validate interactions with the highest coincidence score, we took advantage of a single-molecule two-color coincidence assay (Fig 3F) previously used to determine stoichiometric ratios for SOX18 protein partners (Sierecki *et al*, 2014; Moustaqil *et al*, 2018). In the case of the SOX7 and HEY1 interaction, the coincidence ratio in the same

confocal volume of SOX7-GFP and HEY1-mCHERRY individual molecules was 0.66 (Fig 3F, yellow trace). This ratio defines a stoichiometric relationship of 1:2, indicating two HEY1 molecules recruit one SOX7 molecule. Further validation of SOX7/HEY1 protein recruitment was performed *in vitro* using co-immunoprecipitation experiments in HEK293 and HUVECs cells transiently transfected with epitope-tagged constructs (Fig 3G, Appendix Fig S6). Together, we show that SOX7 is capable of physically engaging with HEY1, and raise the possibility that SOX7 not only indirectly represses *VEGFC* transcription through modulation of HEY1 levels but can also coordinate transcriptional repression through a direct protein recruitment process at *VEGFC* regulatory regions on the genome.

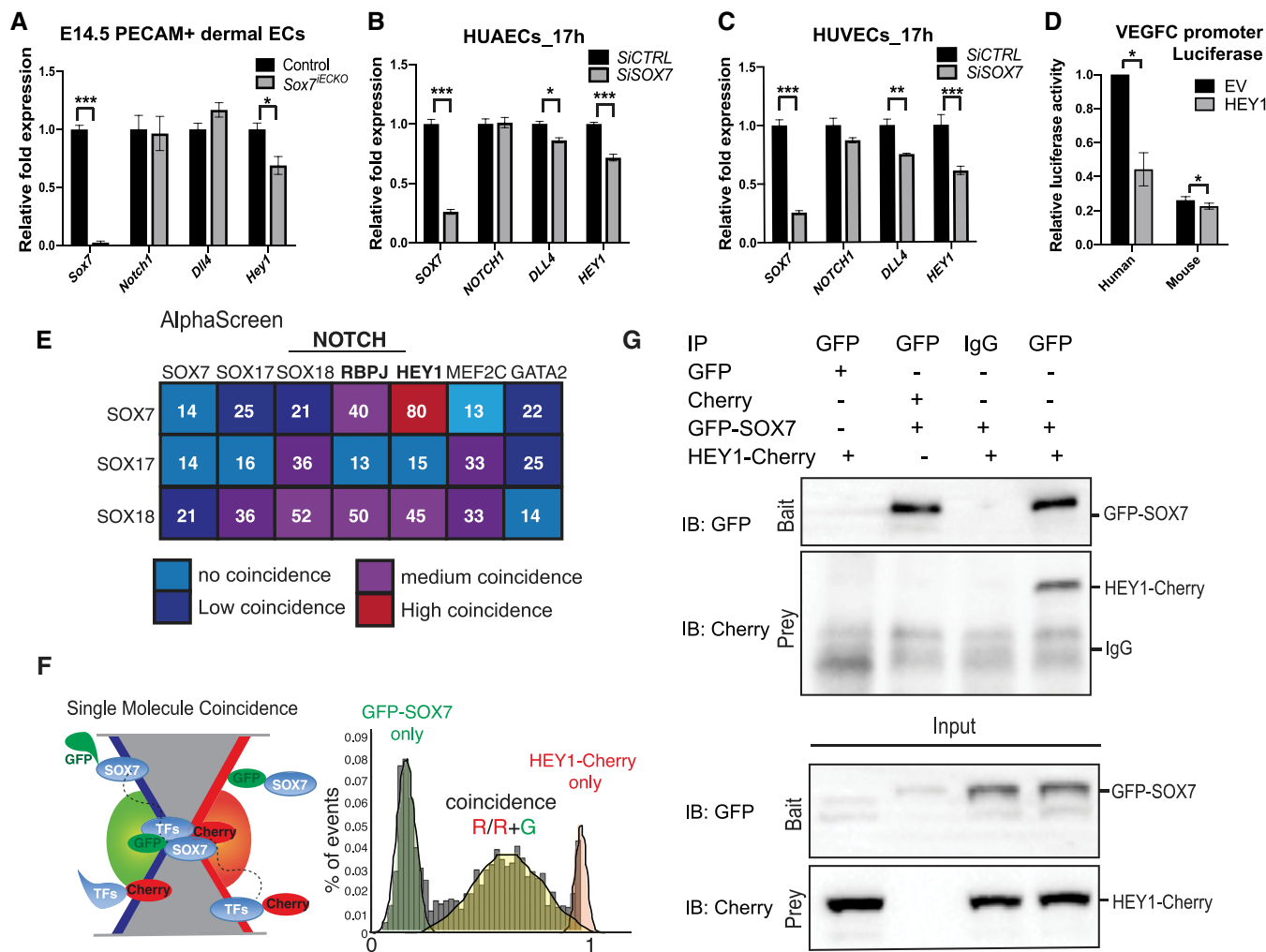


Figure 3. SOX7 indirectly suppresses VEGFC expression through the Notch pathway.

A–D SOX7 transcriptionally activates Notch effector, HEY1, to repress *Vegfc*. (A) qPCR on FAC-sorted PECAM⁺CD45[−] endothelial cells of Sox7^{IECKO} mutants and sibling controls at E14.5 after Cre induction with tamoxifen at E11.5 and E12.5. Expression is normalized to the endothelial markers *Pecam* and *Cdh5*. Scored sibling controls, *n* = 9; Sox7^{IECKO} mutants, *n* = 8. (B, C) qPCR on (B) human arterial endothelial cells (HUAECs) and (C) human venous endothelial cells (HUVECs) transfected with SiSOX7 or SICTRL for 17 h. In addition to HEY1, DLL4 levels were also downregulated in the human cell line experiments. Expression is relative to *HPRT* and *GAPDH*. Data from one siRNA experiment performed in triplicates. (D) HEY1 represses human VEGFC promoter activity. HeLa cells were co-transfected with human or mouse VEGFC-luc and either EV (empty vector) or HEY1 expression constructs as indicated. VEGFC luciferase activity was measured and normalized to Renilla luciferase activity, which was then made relative to the promoter-less vector, pGL3-basic, which was set to 1. Biological replicates, *n* = 3 independent repeats of the same experiment. Mean ± SEM; *t*-test. *P* < 0.05 (*); *P* < 0.005 (**); *P* < 0.0005 (***)

E–G SOX7 physically interacts with transcription repressor, HEY1. (E) Amplified Luminescent Proximity Homogenous Assay (ALPHAScreen) shows the heatmap of SOX7 pairwise protein-protein interaction tested, where red indicates strong interaction and light blue indicates an absence of interaction. (F) Single-molecule spectroscopy reveals that SOX7 is able to directly interact with HEY1. SOX7 and the target transcription factors were tagged with GFP or Cherry. GFP-SOX7 and HEY1-Cherry show coincidence at 0.66, suggesting an interaction with a 1:2 molecular ratio. Peaks centered on 0 (green) or 1 (red) correspond to the GFP or Cherry-tagged proteins only. (G) Co-immunoprecipitation analysis of SOX7 and HEY1. HEK293 cells were transfected with indicated plasmids and harvested 24 h after transfection, immunoprecipitated by anti-GFP or Ig control before immunoblot analysis to determine the presence of bait/prey (top) and the input (bottom). *N* = 2.

Source data are available online for this figure.

SOX7 directly represses VEGFC by acting on its promoter and distal silencing elements

To further investigate the possibility of an alternative mode of SOX7-dependent repression of *VEGFC* gene expression, we next explored the possibility of direct repression of *VEGFC* transcription by SOX7. Using the mouse and human VEGFC promoter luciferase reporter system described above, we assessed the baseline activity

of both constructs either in the absence or presence of SOX7. Surprisingly, SOX7 dramatically suppressed both mouse and human VEGFC promoters (Fig 4A), supporting the notion that SOX7 has the potential to act as a direct negative regulator of *VEGFC* transcription.

This observation suggested that SOX7 might interact with other *VEGFC* regulatory regions more broadly on a genome-wide scale. To probe for SOX7 genome-binding locations, we took advantage of our

SOX7-mCherry ChIP-Seq dataset from human venous endothelial cells (HUVECs) (<https://www.ebi.ac.uk/arrayexpress/experiments/E-MTAB-4480/>) (Overman *et al*, 2017). Analysis of this dataset using the top 2k most intense ChIP-Seq peaks revealed that the VEGF ligand-receptor interaction is one of the top 4 most enriched pathways (Fig EV5A), thereby confirming that SOX7 preferentially binds to regions associated with the VEGF/VEGFR pathways. We identified a putative *VEGFC* regulatory region situated 255 kb upstream from the *VEGFC* transcription start site (TSS), named *VEGFC-255* (Fig 4B). Although the *VEGFC-255* region does not overlap with either active (H3K27Ac) or repressive (H3K9me3, H3K27Me3) histone marks, it coincides with an open chromatin region (as revealed by DNaseI) where the transcription repressor

and insulator CTCF binds (Fig 4B; Filippova *et al*, 1996; Cuddapah *et al*, 2009). Further, chromatin state segmentation analysis (Chrom HMM) from ENCODE confirmed that the binding region *VEGFC-255* has been associated with insulators (purple box) and poised enhancers (green box; Fig 4B). Interestingly, poised enhancers are usually bound by Polycomb Repressive Complex (Pc-R) (Cruz-Molina *et al*, 2017), and we observed a large Polycomb-repressed region situated around ~5 kb upstream from *VEGFC-255* (Pink box, Fig 4B), which might suggest that this region has a repressive function.

To determine whether the putative regulatory elements observed in the human ChIP-Seq dataset are conserved in mouse *in vivo*, we used the *Sox7-V5* reporter line to perform ChIP-Seq analysis in E9.5

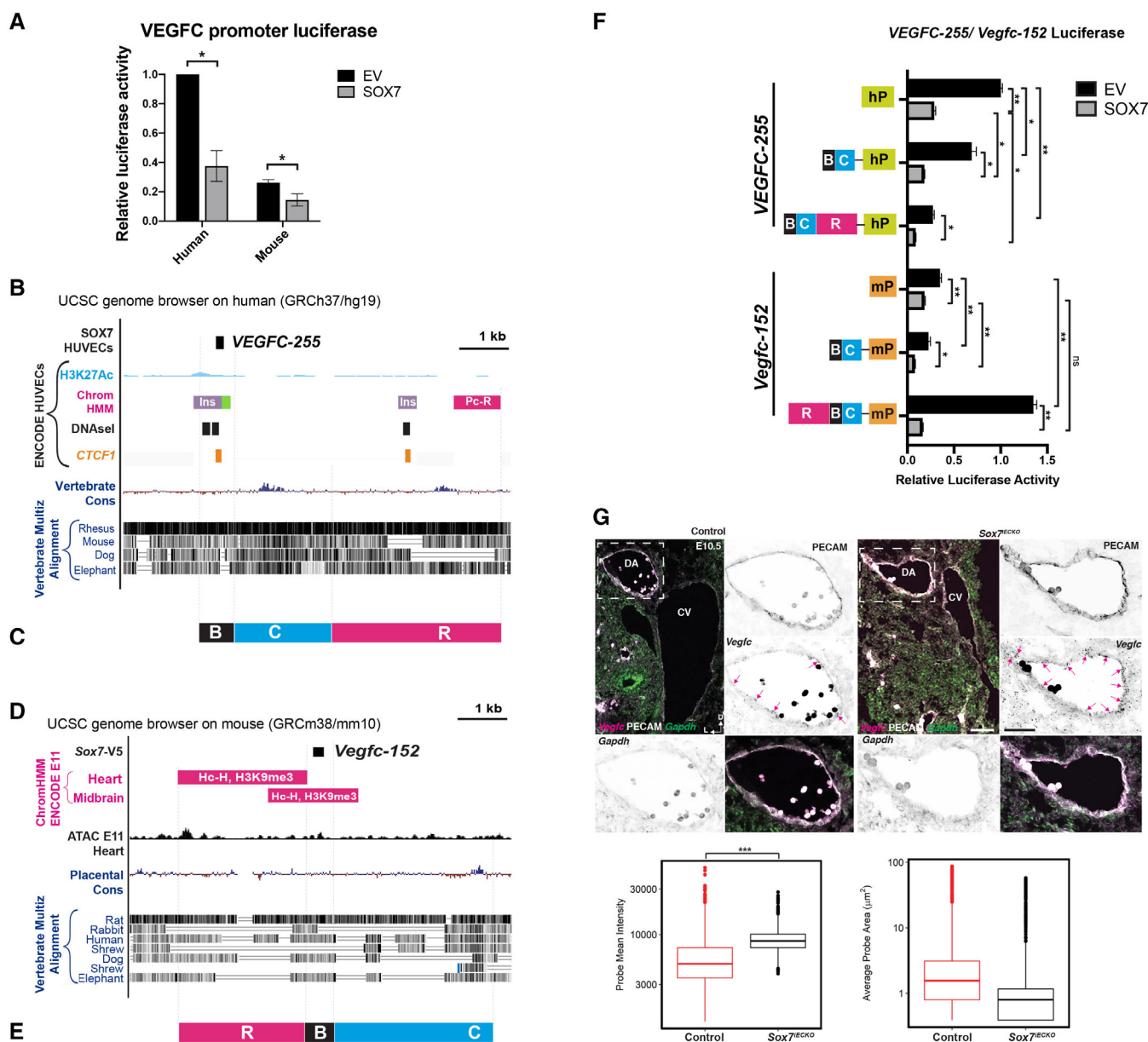


Figure 4.

Figure 4. SOX7 directly binds to silencing regions at the *Vegfc* locus and represses *Vegfc* transcription.

- A SOX7 represses human VEGFC promoter activity. HeLa cells were co-transfected with human or mouse VEGFC-luc, EV (empty vector), or SOX7 expression constructs as indicated. VEGFC luciferase activity was measured and normalized to Renilla luciferase activity, which was then made relative to the promoter-less vector, pGL3-basic, which was set to 1. Biological replicates, $n = 3$. Mean \pm SEM; t-test. $P < 0.05$ (*).
- B Schematic representation of the human *VEGFC* locus 255 kb upstream from the transcription start site (TSS) (denoted as *VEGFC*-255 region) from the UCSC Genome browser. The H3K27Ac is denoted in light blue, and DNaseI hypersensitive hotspots are indicated by black/gray boxes, where the darkness is proportional to the maximum signal strength observed in any cell line. The chromatin state in HUVECs is shown in purple (indicates insulator), green (poised enhancer), and pink (a Polycomb-repressed region). The HUVECs CCCTC-binding factor (CTCF)-binding location is shown in orange. Multiple species conservation is shown in blue peaks and alignments with black stripes.
- C The human luciferase *VEGFC*-255 BCR transgene. B (black), binding region; C (blue), conserved region and R (pink), repressive region.
- D Schematic representation of the mouse *Vegfc* locus 152 kb upstream from the TSS (denoted as *Vegfc*-152). The chromatin state in mouse at E11 from ENCODE is denoted in pink (indicates a heterochromatin region enriched for H3K9me3 repressive marker). The ATAC-Seq (in black) indicates accessible DNA regions in E11 mouse hearts. Multiple species conservation is shown in blue peaks and alignments with black stripes.
- E The mouse luciferase *Vegfc*-152 RBC transgene. R (pink), repressive region; B (black), binding region and C (blue), conserved region.
- F SOX7 represses VEGFC promoter activity through *VEGFC*-255 and *Vegfc*-152. HeLa cells were co-transfected with human or mouse VEGFC-luc, *VEGFC*-255 BC-luc, *VEGFC*-255 BCR-luc, *Vegfc*-152 BC-luc, *Vegfc*-152 RBC-luc, EV (empty vector), or SOX7 expression constructs as indicated. VEGFC luciferase activity was measured and normalized to Renilla luciferase activity, which was then made relative to the promoter-less vector, pGL3-basic, which was set to 1. Biological replicates, $n = 3$. Mean \pm SEM; t-test. $P < 0.05$ (*); $P < 0.005$ (**); ns = not significant.
- G Quantitation of *Vegfc* transcript using single-molecule FISH *in vivo*. (colored panel) Representative low magnification images of the trunk transverse sections of E10.5 sibling controls and *Sox7*^{IECKO} mutants showing the similar relative position of the DA and the CV across genotypes. Sections were stained by single-molecule FISH (smFISH) for *Gapdh* (green) and *Vegfc* (magenta) and immuno-stained for PECAM (white). Individual molecules of *Vegfc* transcript (pink arrows) are detectable within the cytoplasm of PECAM-positive cells of the dorsal aorta (Middle panel). (Left graph) Quantitation of *Vegfc* transcript level in the PECAM-positive endothelial cells of the dorsal aorta, in sibling controls and *Sox7*^{IECKO} mutants at E10.5. The mean gray scale intensity of the *Vegfc* probes in control was 5,845. The mean gray scale intensity of the *Vegfc* probes in *Sox7*^{IECKO} was 8,956. Mean probe intensity was significantly higher in *Sox7*^{IECKO} compared with the control ($P < 2e-16$). (Right graph) No differences were observed for the average probe area, meaning that the distribution of the probes across the dorsal aorta remained unchanged between the control and *Sox7*^{IECKO}. Scored sibling controls, $n = 5$; *Sox7*^{IECKO} mutants, $n = 7$. Mean \pm SEM; t-test. $P < 0.0005$ (***). Graph: box, interquartile range, central band, median, whiskers, indicate maximum and minimum. Scale bars; low magnification 150 μ m, high magnification, 30 μ m.

Source data are available online for this figure.

and E10.5 mouse embryos. This approach identified 12,976 binding regions in E9.5 and 3,351 binding regions in E10.5 embryos (Fig EV5B). In addition to observing the presence of SOX7-binding motifs among the most enriched transcription-binding motifs at both time points (Fig EV5C–E), we further validated this dataset by performing ChIP-PCR on the top 5 most intense peaks and other assumed unbound regions (negative control; Fig EV5F). Gene ontology analysis found GO:0007411 axon guidance and GO:0045499 chemical repellent activities as the top biological process and molecular function in the overlapping genes between E9.5 and E10.5 SOX7-V5 ChIP-Seq (Fig EV5G–J). Pathway analysis further showed that “axon guidance” is the most significant pathway associated with these genes, suggesting that SOX7 may also regulate lymphatic patterning through the modulation of other guidance molecules in addition to VEGFC (Appendix Table S1).

A common feature of the *in vivo* E9.5 and E10.5 ChIP-Seq results and the SOX7 HUVEC ChIP-Seq dataset is the presence of peaks assigned to the *Vegfc* locus. By contrast, we did not detect any binding to regions associated with *Vegf*, *Vegfd*, *Vegfr1*, *Vegfr2*, or *Vegfr3*. At E9.5, SOX7 binds to sites 186 kb upstream (*Vegfc*-186) and 251 kb downstream (*Vegfc*+251) of the VEGFC TSS. At E10.5, SOX7 binds to sites 381 and 152 kb upstream (*Vegfc*-381, *Vegfc*-152) of the VEGFC TSS, suggesting four putative regulatory elements are recruited differentially at distinct embryonic time points. Of these four binding regions, *Vegfc*-152 is associated with a region enriched for the repressive histone mark H3K9me3, typically linked to a constitutive heterochromatin state as revealed by the E11 mouse ENCODE data repository (Fig 4D). Other peaks do not appear to coincide with any of the known histone marks reported in the ENCODE database for E10.5–E11 mouse embryos.

Both *VEGFC*-255 (human) and *Vegfc*-152 (mouse) contain multiple partially conserved SOX- and ETS-binding motifs

(Appendix Fig S7). Identification of SOX7-binding sites in distal regions assigned to *VEGFC* loci, consistently in both human and mouse, suggests that SOX7 might act as a direct transcriptional regulator of VEGFC in both species through these putative distal regulatory elements.

To test whether *VEGFC*-255 and *Vegfc*-152 have any regulatory potential on VEGFC promoter activity, we generated a series of VEGFC luciferase reporter constructs that harbor a combination of different putative regulatory regions from mouse (mP) and Human (hP) (Fig 4C and E, Appendix Fig S7). As a starting point, we used SOX7-chromatin bound regions “B” (black bar, Fig 4C, E and F) in combination with a conserved flanking region “C” (blue bar, Fig 4C, E and F) located in 3’ of the “B” region in both human and mouse. In addition, we also included in these reporter constructs nearby genomic regions labeled by repressive marks referred to as “R” (pink bar, Fig 4C, E and F). The “R” region is located in 5’ of the B element in mouse and in 3’ in human. The largest fragment generated for this series of combinations is made up of all “RBC” regions and is approximately 6.5 kb long.

As noted above, SOX7 repressed both human and mouse VEGFC basal promoter activity (Fig 4A and F). For the human constructs, the addition of the “R” and “B” and “C” regions in all cases led to a decrease in VEGFC basal promoter activity. This repressive effect was further enhanced in presence of SOX7 over-expression (Fig 4F). By contrast in the context of the mouse genome, the “RBC” region caused an increase in VEGFC basal promoter activity; however, SOX7 over-expression led to a marked decrease in the VEGFC reporter activity, similar to what was observed with the human constructs. Taken together, results from this *in vitro* reporter assay support the notion that SOX7 directly represses *Vegfc* transcription via a combination of inhibitory regions, likely involving the coordinated activity of both the VEGFC promoter and distant regulatory

elements. This repressive mechanism appears to be functionally conserved between mouse and human.

As a final demonstration that SOX7-dependent transcriptional regulation is relevant *in vivo*, we measured *Vegfc* transcripts using smFISH comparing control and *Sox7^{iECKO}* embryo at E10.5 (Fig 4G). This analysis shows a significant enrichment of *Vegfc* mRNA in BECs especially in the dorsal aorta (Fig 4G, pink arrows) with *Sox7^{iECKO}* embryo showing significantly higher expression levels (Fig 4G, graphs). This endothelial-specific increase in *Vegfc* transcripts was further validated in *Sox7*-null BEC by taking advantage of smFISH analysis in the *Sox7^{iECKO}*.mT/mG transgenic line, where GFP positive cells show a high level of *Vegfc* mRNA (Appendix Fig S8, pink arrows).

More broadly, the observation that SOX7 loss-of-function leads to *Vegfc* upregulation both *in vitro* and *in vivo*, combined with the identification of SOX7-dependent VEGFC-silencing regions, suggests that direct transcriptional repression of VEGFC is a significant mechanism that regulates the expression of this growth factor in BECs.

Loss of *Sox7* function disturbs the emergence and expansion of LEC progenitors *in vivo* similar to VEGFC gain-of-function

Having already established that BEC-specific loss of SOX7 function in mice causes defects in lymphatic patterning, we next sought to link these defects specifically with VEGFC de-repression. Previous work has established that VEGFC promotes LEC specification and expansion (Mäkinen *et al*, 2001; Srinivasan *et al*, 2014; Pichol-Thievend *et al*, 2018). We therefore hypothesized that the ectopic activation of VEGFC, especially in close vicinity to the CVs at the time of the initial steps of lymphangiogenesis, would change both the distribution and number of PROX1-positive LEC progenitors. To test this hypothesis, we analyzed both the anatomical locations and density of LEC progenitors in the CVs in E11.5 *Sox7^{iECKO}* mutant embryos. During development, PROX1⁺ LEC progenitors are polarized to a dorsal-lateral aspect of the CVs in the anterior part of the embryo (Wigle & Oliver, 1999; Bowles *et al*, 2014). Our analysis revealed an increase in the proportion of PROX1⁺ LEC progenitors in the *Sox7^{iECKO}*, as well as an ectopic distribution of LEC progenitors in the ventro-medial aspects of the CVs (yellow arrowheads, Figs 5A–C and EV2J). Another indirect indication of *Vegfc* increased signal caused by the loss of SOX7 function is the presence of angiogenic blood vascular phenotype at E10.5 (Appendix Fig S9). It has been previously shown by (Lohela *et al*, 2008) that VEGFC over-expression in the endothelium using the *Tie1-TetR-VP16:tetOS-mVegfc* double transgenic animals give rise to lymphatic vessels hyperplasia and angiogenic sprouting defects. In E10.5 embryo, lymphatic vessels have not yet developed, and most blood vessels still express VEGFR3, hence the angiogenic response in presence of *Vegfc* over-expression. In the *Sox7*-null animals, we observed an ectopic sprouting from the dorsal aorta toward the ventro-medial side of the embryo (Appendix Fig S9A, white arrowheads) and ectopic formation of the intersomitic dorsal arteries (Appendix Fig S9B, blue arrows). Further, the immature blood vasculature in the cephalic region also displays excessive angiogenic sprouts (Appendix Fig S9C).

Previously, others and we have shown that the dermal blood capillary network is an ongoing source of the dermal LECs progenitors, and the emergence of these precursor cells from the

endomucin-positive plexus is dependent on CCBE1/VEGFC/VEGFR3 signaling (Martinez-Corral *et al*, 2015; Pichol-Thievend *et al*, 2018). High levels of VEGFC expression in blood vascular endothelial cells increase the number of LECs within the blood capillary plexus, as observed in the *Tie2Cre;VegfcGOF* mice (Pichol-Thievend *et al*, 2018). To investigate whether an increase of *Vegfc* levels in *Sox7^{iECKO}* mutants (as characterized above in Figs 2C and 4G) similarly affects the number of LECs in the dermal capillary, we quantified the number of isolated PROX1-positive LEC progenitors. These progenitors were located either on or within the vessel wall of endomucin-positive blood vessels in E12.5 skin (Fig 5D and E, Appendix Fig S10). Our quantitative analysis focused on EMCN^{low/-}PROX1⁺NRP2^{+/low} individual LECs (arrowhead, type I) on blood vessels, EMCN⁺PROX1⁺NRP2^{low/-} LECs within the vessel wall (arrow, type II) and EMCN^{+/-}PROX1⁺NRP2^{+/low} LEC clusters (2–4 cells, empty arrowhead, type III) that were exiting from the blood plexus network. Similar to the *Tie2Cre;VegfcGOF* embryonic skin (Pichol-Thievend *et al*, 2018), analysis of *Sox7^{iECKO}* skin revealed a significant increase in the number of PROX1⁺ LEC progenitors associated with the blood plexus (Fig 5E, Appendix Fig S10C–E).

Taken together, the increase of LEC specification events in the CVs and the dermal blood capillaries correlated with higher levels of *Vegfc* transcripts in SOX7 mutants *in vivo* establishes SOX7 as a key BEC-specific regulator of lymphatic vessel patterning through negative modulation of VEGFC expression.

Discussion

While it is well-established that SOX7 acts in a cell-autonomous manner to instruct angiogenesis and arterio-venous specification during development (Hermkens *et al*, 2015; Kim *et al*, 2016; Lilly *et al*, 2017), this study reveals for the first time a function for this BEC-specific transcription factor in regulating signaling crucial for the organization of the lymphatic vasculature. We show that one mechanism by which SOX7 achieves this role is via the transcriptional repression of *Vegfc* in the blood vascular endothelium. This fine tuning of VEGFC local repression is required to maintain strict control over the number and spatial distribution of LECs essential for the correct assembly of the dermal lymphatic vascular network.

To date, only a handful of factors have been shown to transcriptionally regulate VEGFC expression (Schuermann *et al*, 2015; Gauvrit *et al*, 2018; Cohen *et al*, 2020), with no previous study describing an endothelial-specific and direct molecular mechanism that regulates VEGFC transcription. Our work sheds light on how the BEC-specific SOX7 transcription factor dampens local VEGFC levels to modulate tissue growth in a paracrine manner likely via a combination of mechanisms: (i) indirectly through recruitment and transcriptional control of the repressor protein HEY1 (ii) directly via binding to silencing elements associated with the *Vegfc* locus.

Conventionally, within the context of embryonic development, the SOXF (7, –17, and 18) transcription factors have been shown to act mainly as transcriptional activators (Chew & Gallo, 2009). Unlike the SOXB2 transcription factors (SOX21 and SOX14) that possess a repression domain, SOXF proteins have a transactivating domain (Uchikawa *et al*, 1999; Schock & LaBonne, 2020). Similar to SOX18 and SOX17 (Hosking *et al*, 2004; François *et al*, 2008; Corada *et al*, 2013), SOX7 has primarily been reported to positively regulate

gene transcription (Futaki et al, 2004; Murakami et al, 2004; Niimi et al, 2004; Costa et al, 2012; Sacilotto et al, 2013; Kim et al, 2016; Chiang et al, 2017), although there have been a handful of reports of SOX7 acting to repress transcription via the sequestration of activators through direct protein-protein interaction (Guo et al, 2008; Lilly et al, 2016; Fan et al, 2018). Other repressive mechanisms are

possibly at play such as an indirect regulatory cascade whereby SOX7 loss-of-function causes a failure to activate a repressor such as HEY1, which in turn causes an activation of downstream target genes. It is also possible that the DNA environment and the code of binding co-factors turn an activator into a repressor, as exemplified by a Drosophila morphogen, Dorsal (Ip, 1995). Here, we show that

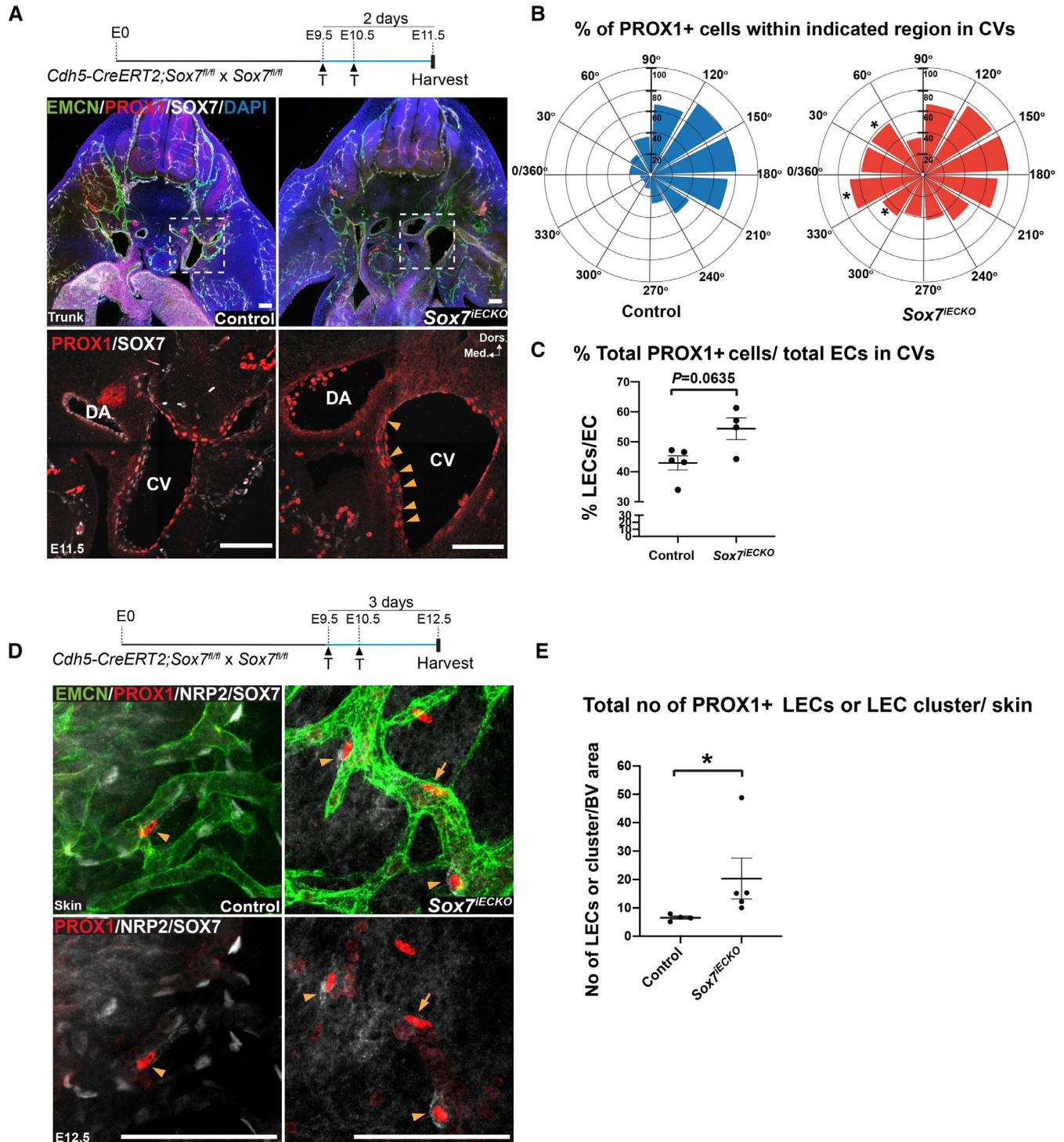


Figure 5.

Figure 5. Loss of SOX7 transcription factor function causes ectopic LEC localization in the cardinal veins and an excess of local LEC progenitors in embryonic skin.

- A At 2 days post-Cre induction, E11.5 *Sox7^{IECKO}* mutants showed ectopic expression of PROX1⁺ (red) in medial ventral regions of the cardinal veins (CVs), close to dorsal aorta (DA) (yellow arrowheads).
- B Rose diagram indicates the % of PROX1⁺ cells over the total number of EMCN⁺ endothelial cells, within each indicated region. The medial region closest to the DA is indicated by 0/360°; most lateral region, 180°; dorsal, 90° and ventral, 270°. Scored sibling controls, *n* = 5; *Sox7^{IECKO}* mutants, *n* = 4. Mean ± SEM; Mann–Whitney *U*-test. *P* < 0.05 (*).
- C Graph indicates the % of total PROX1⁺ cells over the total number of EMCN⁺ endothelial cells within each embryo analyzed. A total of 2,907 endothelial cells quantified, from *n* = 5 sibling controls and 1,780 endothelial cells from *n* = 4 *Sox7^{IECKO}* mutants. Mean ± SEM; Mann–Whitney *U*-test. *P* = 0.0635.
- D Whole-mount immunostaining of control and *Sox7^{IECKO}* embryonic skin at E12.5 after *Cre* induction at E9.5, E10.5. Dermal lymphatic structures are stained with NRP2 (membranous white), lymphatic endothelial cells, PROX1 (red), and blood vessels, both EMCN (green) and SOX7 (white nuclei). Arrowheads indicate EMCN^{low/}PROX1⁺NRP2^{+/low} individual LECs on blood vessels (type I), and arrow shows EMCN⁺PROX1⁺ NRP2^{low/} LEC within the vessel wall (type II).
- E Graph shows the total events of PROX1⁺ single LECs or LEC clusters cells associated with EMCN⁺ blood vessel plexus within each embryo. PROX1⁺ cells were quantified from *n* = 4 controls and *n* = 5 *Sox7^{IECKO}* mutants. Mean ± SEM; Mann–Whitney *U*-test. *P* < 0.05 (*).

Data information: Dors.—dorsal; Med.—medial. Scale bars = 100 μm.

Source data are available online for this figure.

repression of *Vegfc* transcription by SOX7 may involve indirect mechanisms mediated by the modulation of Notch signaling effector activity, but importantly, we also uncover a novel mechanism involving direct recruitment of SOX7 to silencing elements associated with the *Vegfc* locus.

In terms of indirect regulation of VEGFC expression by SOX7, while this study has not definitively defined the role of SOX7-HEY1 interaction in the context of VEGFC transcriptional regulation, our data provide compelling evidence to explore this interaction further. It is possible that SOX7 may induce HEY1 gene expression to promote the assembly of a SOX7/HEY1 heterodimer that in turn represses VEGFC as part of a positive feedback loop. Notably, we detected two HEY1-binding motifs 5'-CACGTG-3' in human VEGFC-255 RBC and a single HEY1-binding motif in the human VEGFC promoter (data not shown). Although the SOXF and HEY1-binding sites are far apart, physical interaction could be made possible through changes in chromatin conformation. In addition, it is possible that SOX7 recruitment of its protein partner does not involve direct HEY1/DNA interaction. Importantly, this study supports a previous report on the importance of Notch signaling in the negative regulation of LEC specification and expansion (Murtomaki *et al*, 2013), and begins to unravel the potential role of SOX7 in mediating this regulation. We propose that SOX7 and Notch/HEY1 may function as converging pathways, to produce a combinatorial effect on *Vegfc* repression in order to maintain LEC progenitor homeostasis.

In parallel to the indirect regulation of *Vegfc* by SOX7, our study identified putative VEGFC-silencing elements in both the human and mouse genomes and suggested that SOX7 can regulate *Vegfc* transcription through direct binding at these sites. While a handful of factors have been shown to transcriptionally regulate VEGFC expression in the past (Schuermann *et al*, 2015; Gauvrit *et al*, 2018; Cohen *et al*, 2020), this is the first identification of an endothelial-specific and direct molecular mechanism able to regulate *Vegfc* transcription.

As previously described, silencing elements are enriched in the H3K9me3 mark and H3K27me3 mark, which are associated with Polycomb repression (Pang & Snyder, 2020). Deletion of Polycomb-bound elements was recently shown to lead to the de-repression of their target genes, inferring that Polycomb-bound regions could potentially function as silencers (Ngan *et al*, 2020). Having identified a number of SOX7-binding sites associated with the VEGFC

genomic locus, *in silico* evaluation of the chromatin states of the VEGFC-255 and *Vegfc*-152 regions revealed characteristics of silencing elements. We further substantiated these *in silico* observations by demonstrating the ability of these genomic regions to reduce VEGFC promoter activity *in vitro* when fused to luciferase synthetic constructs. The presence of insulator CTCF and Polycomb repressor-binding sites in VEGFC-255 suggest a possible direct or indirect molecular relationship between SOX7 and CTCF or Polycomb repressing complexes to elicit repression. Interestingly, both CTCF and CTCFL (BORIS) are among the top enriched secondary binding motifs in SOX7 HUVEC ChIP-Seq (Appendix Fig S11A). Further, overlapping of the SOX7 HUVEC and V5 ChIP-Seq data with histone marks from the ENCODE consortium reveals a large proportion of the peaks have at least 50% overlap with a repressive mark (H3K27me3 or H3K36me3) further supporting a repressive mode of action for SOX7 (Appendix Fig S11B–L). Analysis of the chromatin state of the SOX7 HUVEC ChIP-Seq reveals most peaks are associated with heterochromatin, followed by strong enhancers and weakly transcribed regions (Appendix Fig S11F). Interestingly, 4.7% of the peaks are found associated with Polycomb-repressed regions.

A repressive function has been implicated for at least one other SOXF transcription factor; with SOX18 homodimer-binding motifs (inverted repeat-5, IR-5) found associated with both active and repressive histone marks (Moustaqil *et al*, 2018). SOX7 repressive effects on *Vegfc* transcription in the CVs and dermal blood plexus could potentially act as a “shield” to maintain some LEC-free areas, therefore preserving vessel integrity and function (see model, Fig 6). Nonetheless, it is unlikely that the SOX7 lymphatic defects are solely relying upon an upregulation of VEGFC level restricted to the blood endothelium compartment. Identification of multiple putative guidance cues previously implicated in LEC migration and patterning such as semaphorins, netrin receptors, and ephrins in SOX7-V5 ChIP-Seq data further suggested that dysregulation of these guidance cues could also contribute to the overall migration defects observed in the lymphatic network (Appendix Table S1) (Uchida *et al*, 2015; Liu *et al*, 2016). It is also important to consider other heterotypic interactions such as endothelial-to-mesenchymal cell interplay. The loss of SOX7 function seems to cause an increase of *Vegfc* in the mesenchyme located at the dorso-lateral region of the cardinal vein. It is therefore likely that BEC to mesenchymal cell interaction indirectly influences the patterning of the lymphatics. Further, VEGFC processing molecules such as CCBE1 might also be involved to

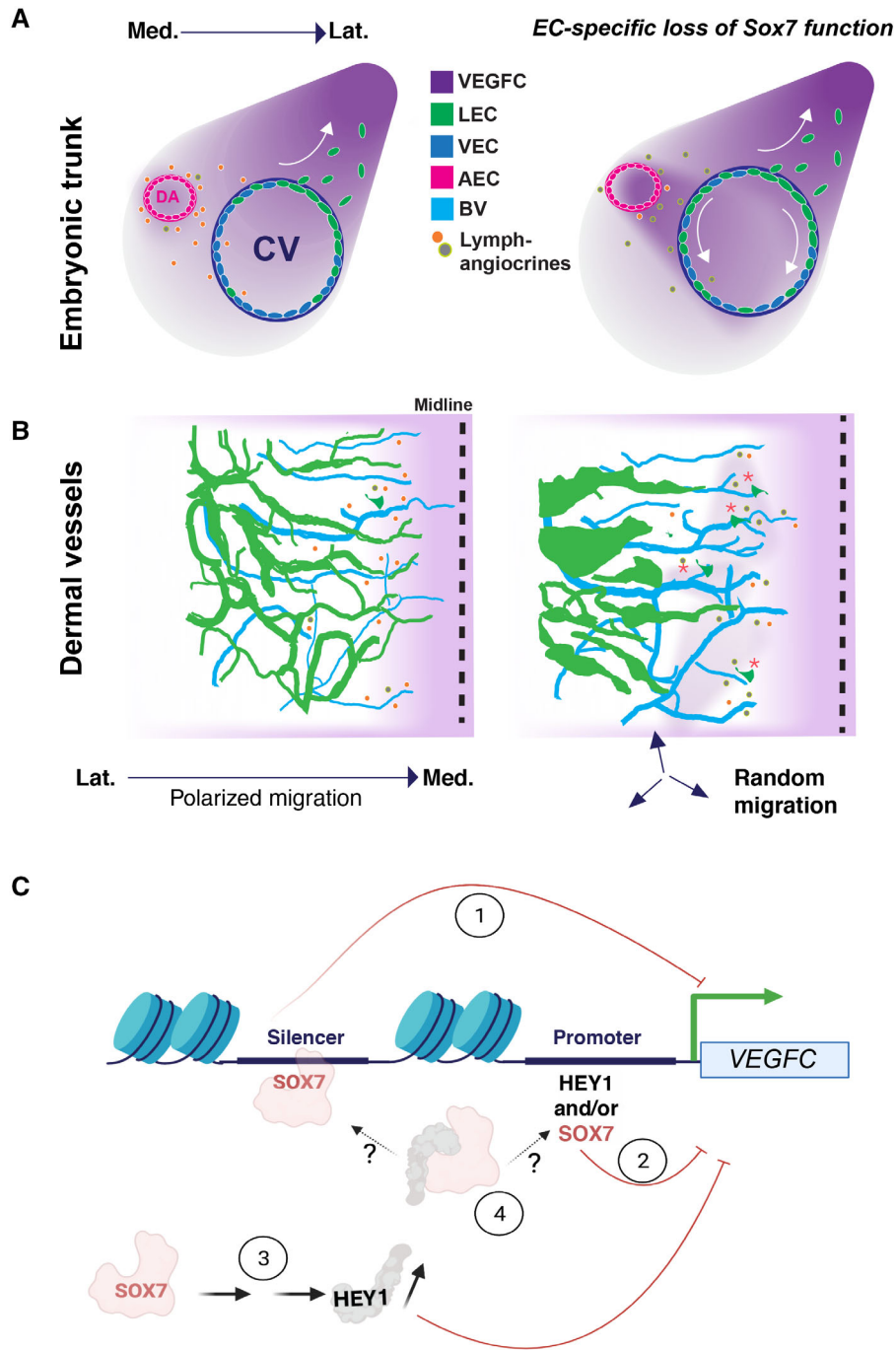


Figure 6. Model depicting how the loss of SOX7 function in blood vascular endothelial cells causes defective lymphatic vascular patterning.

A, B LEC progenitor organization is impaired in both early-stage and organ-specific lymphangiogenesis. (A) In physiological conditions, LEC progenitors emerge in the dorsal-lateral part of the CVs and migrate toward the dorso-lateral aspects of the embryo. In the absence of functional SOX7, blood vascular endothelial cells from the arterial compartment increase the local expression of endothelial VEGFC, perturbing its tissue distribution. This induces and/or expands the number of LEC progenitors in ventro-medial aspects of the CVs. (B) Dermal lymphatics are dysmorphic in the absence of SOX7 function in blood vascular endothelial cells. An increase in VEGFC in the dermal blood endothelial cells causes hyperproliferation of local LEC progenitors. This is shown by an increase in the emergence of local LEC progenitors from the endomucin-positive blood capillary plexus at E12.5 (red asterisks). Changes in expressions of other SOX7-dependent angiocrines also contribute to the migration defects in the dermal lymphatics.

C Model showing the molecular mechanisms of SOX7-dependent repression of VEGFC transcription identified in this study: (1) SOX7 binds to distal regulatory elements (silencing regions) to suppress VEGFC transcription. (2) SOX7 represses VEGFC promoter activity. (3) SOX7 acts upstream of Notch effector and repressor, HEY1. SOX7-induced expression of HEY1 causes VEGFC downregulation and (4) Protein-protein interaction between SOX7 and HEY1 forms a complex to repress VEGFC transcription. AEC, arterial endothelial cells; Lat., lateral; LEC, lymphatic endothelial cells; Med., medial; VEC, venous endothelial cells.

indirectly regulate the morphogenetic signal from the blood vascular compartment.

Whether SOX7 functions as an activator or a repressor in a given context is likely to be dictated by the surrounding chromatin state, as well as the spatial and temporal distribution of its binding co-factors (Ip, 1995). Like the CRX transcription factor in rod photoreceptors, the SOX7 dual function as activator or repressor might also be dependent on the number and affinity of its binding sites at particular regulatory elements (White *et al*, 2016). Given the known role of SOX7 to maintain endothelial cell identity and repress the hemogenic program (Gandillet *et al*, 2009; Lilly *et al*, 2016), it is highly likely that the coordinated activity of activating and repressive function are at play in the same cell at the same time for a specific subset of gene regulatory network.

By uncovering a number of novel mechanisms by which SOX7 can modulate *Vegfc* transcription, this study reveals that the final transcriptional output of VEGFC in BECs is likely to involve a complex interplay of molecular events exquisitely coordinated in a strict spatio-temporal manner. Our data suggest that while SOX7 alone appears sufficient to reduce VEGFC promoter activity, it is likely that *in vivo* SOX7 works in concert with other co-factors at different distal regulatory elements to effectively coordinate changes in *Vegfc* transcription rate. We demonstrate that this BEC-specific SOX7/VEGF-dependent regulatory axis, potentially with other unidentified SOX7-regulated angiocrines, is essential for appropriate LEC specification and spatial organization into a functional lymphatic network; further cementing the role of the blood vascular network in guiding lymphangiogenesis.

Materials and Methods

Mice and breeding

All animal work conformed to ethical guidelines and was approved by the relevant University of Queensland and the University of Sydney ethics committee. The following mice used in this study have been reported previously: *Sox7:tm1* (Chiang *et al*, 2017), *Cdh5-CreERT2* (Wang *et al*, 2010), *Prox1-CreERT2* (Srinivasan *et al*, 2007), *Sox7^{fl/fl}* (Lilly *et al*, 2017), and *mT/mG* (Muzumdar *et al*, 2007). The *Sox7-V5* tagged mice (mixed background) were generated as detailed in [Materials and Methods](#). The *Sox7* endothelial-specific conditional knockout, *Cdh5-CreERT2:Sox7^{fl/fl}*, was crossed between *Cdh5-CreERT2* and *Sox7^{fl/fl}*. All mice strains were in C57BL/6 genetic background.

To delete *Sox7* specifically in endothelial cells, each pregnant dam received two consecutive intraperitoneal injections of tamoxifen (T5648, Sigma Aldrich), at 1.5 mg per pulse at the indicated time point. Tamoxifen was reconstituted in 10% (v/v) ethanol and 90% (v/v) peanut oil.

Chromatin immunoprecipitation (ChIP) sequencing

Homozygous *Sox7-V5* mouse embryos confirmed by sequencing and PCR genotyping were collected at E9.5 and E10.5 and processed as detailed in [Materials and Methods](#) (Mohammed *et al*, 2013). DNA amplification was performed using TruSeq ChIPseq kit (Illumina, IP-202-1012), following an immunoprecipitation step using 10 µg V5

monoclonal antibody (R960CUS, Invitrogen). The library was quantified using the KAPA library quantification kit for Illumina sequencing platforms (KAPA Biosystems, KK4824), and 50 bp single-end reads were sequenced on a HiSeq2500 following the manufacturer's protocol. FASTQ files were mapped to mouse the reference genome Genome Reference Consortium (GRC) m38/mm10 (released in Dec 2011) using Bowtie2 (Galaxy version 2.2.6.2) (Langmead & Salzberg, 2012). Peaks were called using MACS version 2.1.0 (Zhang *et al*, 2008). Potential binding regions of SOX7 (or peaks) were called using each corresponding input DNA as a reference, with a false discovery rate (FDR) of 0.01. Sequencing was performed by the IMB Sequencing Facility, University of Queensland. Please refer to [Materials and Methods](#) for more details.

Tissue sectioning and immunofluorescence staining

For tissue sectioning, whole embryo analysis, and whole-mount immunostaining of embryonic skin, whole embryos were fixed in 4% (w/v) paraformaldehyde/PBS overnight at 4°C and washed three times in PBS. Whole-mount immunofluorescence staining of embryonic skin was performed as described (Pichol-Thievend *et al*, 2018). For sectional analysis, embryos were embedded in 4% agarose and sectioned transversely at 150 µm using the Leica VT1000 S vibrating microtome. For paraffin sectioning, fixed embryos were dehydrated and cleared with a tissue processor (Leica Biosystem). Embryos were then embedded in paraffin before being sectioned (8 µm) with a microtome (Polanco *et al*, 2010). Sections were next rehydrated and boiled in appropriate antigen retrieval solution (Vector) before blocking with blocking solution. This was followed by primary and secondary antibody incubation as described (Pichol-Thievend *et al*, 2018). Details about antibodies can be found in [Materials and Methods](#).

Co-immunoprecipitation and western blotting

At 48 h post-transfection, HEK293 cells were rinsed with PBS before lysis and protein extraction with NE-PER Nuclear and Cytoplasmic Extraction Reagents (Pierce). Protein concentration was measured with Bicinchoninic Acid (BCA) assay (Pierce). To prevent protein degradation, cOmplete Protease Inhibitor Cocktail (Roche, 11697498001) was added to the cell lysate. Clarified nuclear fractions containing the HEY1 and SOX7 were then incubated with anti-GFP (3E6) (1:1,000, A-11120, Thermo-Scientific) or random IgG bound magnetic Dynabeads for 2–3 h, at 4°C with rotation. Beads were then washed three times in RIPA lysis buffer on a magnetic stand, then eluted in SDS sampling buffer with heating for 5 min, before analysis by 12% SDS-PAGE. Immunoblotting was performed with chemiluminescent HRP detection (Pierce) using a ChemiDoc™ Imaging Systems (Bio-Rad). Pull-down and immunoblotting assays were modified from (Schmidt *et al*, 2009). Details about antibodies can be found in [Materials and Methods](#).

Fluorescent Activated Cell sorting (FACS) and expression analysis

CD31⁺CD45⁻ endothelial cells were isolated from skin flaps of E14.5 sibling controls and *Sox7^{iECKO}* mutants (treated with tamoxifen at E11.5, E12.5) (Kazenwadel *et al*, 2012). RNA was extracted and amplified, and cDNA was synthesized as previously described

(Chiang *et al.*, 2017). Primer sequences and details of the qPCR analysis are provided in the [Materials and Methods](#).

Cell-culture and siRNA-mediated silencing experiment

Human umbilical arterial endothelial cells (HUAECs) (C-12202, PromoCell) and human umbilical venous endothelial cells (HUVECs) (CC-2519A) were maintained in EGM2 media (Lonza). For siRNA, Smartpool: ON-TARGETplus Human SOX7 (83595) siRNA 50 nM (containing a mixture of 4 siRNAs against SOX7) (Dharmacon) and scrambled siRNA (Dharmacon) were used. HUVECs and HUAECs were transfected at ~40–50% confluency, using Lipofectamine™ 3000 (Invitrogen) in OptiMEM media. Cells were harvested for RNA extraction at 30 or 17 h post-transfection.

HEK293 cells were maintained in DMEM added with 10% FCS and 1% Penicillin/Streptomycin. HEK293 cells for co-immunoprecipitation assays were transfected for 6 h and incubated for another 18 h before harvesting. DNA transfection was performed using X-tremeGENE™ 9 DNA transfection reagent (Roche) in OptiMEM media according to the manufacturer's instructions.

Imaging and data analysis

Images were captured using a Zeiss LSM710 META BIG, Zeiss LSM 710 FCS, Zeiss LSM-800, or Leica TCS SP8 HyD confocal microscopes with the 10×, 20×, or 40× oil objectives. Images were analyzed with Zeiss Zen software, the Bitplane IMARIS suite, and Image J/FIJI. All graphs and statistical tests were performed with GraphPad Prism 8 and illustrated with Adobe Illustrator CS6. Details about quantification can be found in Materials and Methods. Imaging was performed in the Australian Cancer Research Foundation (ACRF)'s Dynamic Imaging Facility at the Institute for Molecular Bioscience (University of Queensland) and the Sydney Cytometry facilities at Centenary Institute (University of Sydney).

Mice and generation of Sox7-V5

All animal work conformed to ethical guidelines and was approved by the relevant University of Queensland ethics committee.

The *Sox7:tm1* embryonic stem cells were generated using BAC recombination and then injected into C57BL/6 blastocysts (Knock-out Mouse Project [KOMP] repository, US). The *Sox7:tm1* has the entire *Sox7* HMG domain in exon 1 and part of the exon 2 displaced by a *lacZ* cassette. The resulting *Sox7^{+/−}* carriers were crossed to generate *Sox7^{−/−}* embryos.

To identify *Sox7^{fl}* progeny of *Cdh5-CreERT2:Sox7 fl/fl* line, genotyping primers were:

mSox7fl_F: 5'-GGGTTACCGCACTTAAGAGACA-3'
mSox7fl_R: 5'-GGAAGTCTACCGACCTAATC-3'

Wild-type band was 195 bp, flox band was 345 bp.

To identify *Cdh5-CreERT2* progeny, genotyping primers were:

Cre_F: 5'-CTGACCGTACACAAAATTTGCCTG-3'
Cre_R: 5'-GATAATCGCGAACATCTCAGGTTTC-3'

Cre positive band was 200 bp.

Sox7-V5 tagged mice were generated by CRISPR according to the published protocol (Yang *et al.*, 2013) using the following primer and donor oligo:

Sox7-CRISPRgRNA1: 5'-GCTACAGTGTGCATAGAGC-3'

Sox7-V5 donor oligo (V5 tag = underlined):

5'-AGCCTCATCTCAGTCTGGCTGATGCCACGGCCACGTATTACAA
CAGCTACAGTGTGTCAGGCAAGCCCATCCCCAACCCCTGCTGGG
CCTGGACAGCACCTAGAGCTGGAGGAATGGAGCCTGCCAGCC
TGCCATCCCCTCCTCCATGAAGCACT-3'

CBB6F1/BCB6F1 females (CBA x C57BL/6) and Arc:Arc(S) females were used as embryo donors and foster mothers, respectively. Super-ovulated CBB6F1/BCB6F1 females were mated to CBB6F1/BCB6F1 studs, and fertilized embryos were collected subsequently from the oviducts. CRISPR injection mix (containing 10 ng/μl of Cas9 mRNA, 5 ng/μl of gRNA1, and 20 ng/μl of donor oligo) was injected into the pro-nuclei of fertilized eggs. The injected zygotes were cultured in KSOM/M16 media at 37°C, 5% CO₂ until a two-cell stage. Subsequently, 15–25 two-cell zygotes were transferred into the uterus of pseudo-pregnant Arc:Arc(S) at 0.5 dpc.

Genotyping primers for *Sox7-V5* were:

Sox7-V5_SF: 5'-TCACACCTAGTCCCCTCCAC-3'
Sox7-V5_SR: 5'-GTGGGGTTTTGCCAGTTAGA-3'
Sox7-V5_V5R: 5'-TCCAGCTCTAGGTGCTGTCC-3'

For SF/SR primer pairs:

The wild-type allele corresponds to a band at 820 bp, V5 band was 862 bp.

SF/V5R primer pairs

V5 positive band was 479 bp

Nuclei isolation for snRNA-Seq

Skins from E14.5 wild-type mouse embryos were dissected, and snap-frozen in liquid nitrogen before being stored in −80°C freezer. Skins from 3 separate embryos were pooled, and single nuclei were extracted and isolated. Briefly, skins were homogenized in chilled nuclei EZ lysis buffer (N3408, Sigma Aldrich) using a 1 ml douncer, suspended with a wide bore tip before passing through a 70 μm cell strainer (352350, Falcon). Nuclei were washed and resuspended in PBS buffer containing 1% BSA, 0.2 U/μl RNase inhibitor (10777019, Invitrogen), stained in 10 μg/ml DAPI, and passed through a 40 μm cell strainer (352340, Falcon). Nuclei were then sorted using BD FACSAria III with 70 μm nozzle, before being loaded onto the 10X Chromium single-cell chip (v3, 10X Genomics).

Bioinformatic analysis of single-nuclei RNA-Seq

Single nuclei were loaded onto 10× Chromium platform for single nucleus gene expression assay and the snRNA-seq library was sequenced on Illumina NovaSeq 6000. The raw sequencing data were processed using Cell Ranger (version 3.1.0; Zheng *et al.*, 2017), which takes care of read quality control (QC), demultiplexing, genome alignment, and quantification. The resulting count matrix with the dimension number of barcodes × number of transcripts

was obtained and loaded in R (version 4.0.4) for downstream analysis using Seurat (version 4.0.3) (Butler *et al*, 2018), including the selection and filtration of nuclei based on QC metrics, normalization, and variance stabilization of molecular count data using *sctransform*, dimensionality reduction by principal component analysis and Uniform Manifold Approximation and Projection embedding, and clustering analysis.

In the step of QC, nuclei expressing < 200 genes or with genes that were expressed in < 3 cells were filtered. In addition, nuclei were further assessed based on the following criteria: the ones that have > 5% mitochondrial counts and expressed < 200 or > 3,500 unique genes were excluded. This results in 8,380 quality cells. In the step of clustering analysis, the top 30 principal components were used as input. At a resolution of 0.8, 26 clusters were retrieved and projected onto UMAP plots. Following clustering analysis, genes differentially expressed in each of the clusters were determined using a method of differential expression analysis based on the nonparametric Wilcoxon rank-sum test, and genes were filtered based on a minimum log₂ fold change (0.25) for the average expression of gene in a cluster relative to the average expression in all other clusters combined. The top 30 genes were used for cell type annotation. Visualization of expression patterns of specific genes across clusters was performed with Nebulosa in Seurat (Alquicira-Hernandez & Powell, 2021).

Microarray samples

Embryonic mouse LECs and BECs were purified from E14.5, E16.5, and E18.5 skin as previously described (Kazenwadel *et al*, 2010). Each sample was generated from 15 to 21 embryos (pooled from multiple litters) and three independent samples were generated for each time point. Between 0.5 and 3 μg of total RNA were isolated per sample using TRIzol reagent (Thermo Fisher), according to the manufacturer's directions. RNA quality was assessed using a Bioanalyser (Agilent Technologies); all samples achieved an RNA Integrity Number (RIN) score > 9.5. Samples were submitted to the ACRF Cancer Genomics Facility (Adelaide, Australia) and hybridized to GeneChip® Mouse Gene 1.0 ST arrays (Affymetrix) for gene expression profiling. Microarray data analysis was performed using Partek Genomics Suite™ version 6.4 software (Partek Incorporated, St. Louis, MO). Differential gene expression was assessed by one-way ANOVA, with *P*-values adjusted for multiple testing using a step-wise false discovery rate correction (Benjamini & Hochberg, 1995).

Fluorescent RNA *in situ* hybridization

Embryonic tissue sections cut at 10 μm thickness were processed for fluorescent RNA *in situ* hybridization using the commercially available HCR RNA-FISH (Molecular Instruments) or RNAscope® Multiplex Fluorescent v2 assays (Advanced Cell Diagnostics [ACD]) according to the manufacturer's protocols for fresh frozen samples. For the detection of *Vegfc* and *Gapdh*, RNA expression probes from Molecular Instruments were created from accession numbers NM_009506.2 and NM_008084, respectively. Detection was performed using HCR amplifiers conjugated to AF488 and AF647. For the detection of *Vegfc* RNA expression, the Mm-Vegfc-C2 probe (Cat No. 492701-C2; ACD) was used. Detection was performed using the Opal™ 620 dye (FP1495001KT, Perkin Elmer) at a final

concentration of 1:750 in TSA buffer provided in the RNAscope® Multiplex Fluorescent v2 kit.

For subsequent immunostaining, the sections were rehydrated in PBS, then permeabilized in 0.5% Triton X-100 in PBS (PBS-T) followed by blocking in PermBlock (3% BSA, 0.5% Tween-20 in PBS) and incubation with primary antibody diluted in PermBlock at 4°C. Following 3 washing steps with PBS-T, tissues were incubated in secondary antibodies labeled with Alexa-dyes (Life Technologies) at 4°C. After 3 washing steps with PBS-T, the sections were mounted with Mowiol. The following antibodies were used: goat polyclonal anti-human PROX1 (AF2727, R&D Systems), rat monoclonal anti-mouse PECAM-1 (clone 5D2.6 and clone 1G5.1; Wegmann *et al*, 2006) and rabbit anti-GFP (ab6556, Abcam).

Stained embryonic tissue sections were imaged on a Zeiss LSM-800 microscope using a 20x objective NA 0.8. Detectors include two GaAsP PMTs.

smFISH Image batch analysis

Quantification of *Vegfc* was performed on custom Python script.

Briefly, each .CZI image was loaded into python and the channels split. The endothelial cell membranes were identified by firstly running a background subtraction, Gaussian blur, and median filter on the relevant channel. Following this, an "isodata" threshold was performed to make a binary image then small objects were removed. The binary image was then labeled (i.e., objects that are not touching become assigned as unique labels). Probes were identified by running a background subtraction on the relevant channel and then making a binary image using an "otsu" threshold. Red blood cells were isolated by removing all objects smaller than 75 pixels. Individual probes were then identified using watershed. All data presented were acquired using these masks/labeled images to extract relevant mean intensities from the original images. The .CZI images used for smFISH quantitative analysis can be found at <https://doi.org/10.5281/zenodo.7430767>.

Mesentery vessel imaging and quantification

Mesentery was collected from E16.5 mice. After 4% PFA fixation, the whole mesentery was dissected and used to perform whole-mount immune staining as described above for embryonic skins. The mesentery was stained to endomucin (vein) and neuropilin-2 (lymphatics). Mesentery z-stacks were imaged on a Zeiss LSM-800, by stitching together multiple regions per vessel area. Acquisition was done using a 20× objective, NA = 0.8, and using two GaAsP PMTs.

Analysis of mesentery was performed using ImageJ for ROI extraction and Imaris (Oxford Instruments), to create surfaces of both vein and lymphatic vessels. After surface creation, Imaris was used to generate vessel characteristics for quantification.

Graphing and statistics were performed on Prism (Graphpad).

Generation of expression and luciferase constructs

Expression constructs

To generate the expression constructs for co-immunoprecipitation assays, the human SOX7 and HEY1 full-length regions were amplified from a human cDNA library generated in-house from HUVECs. To generate GFP-SOX7, we used the following primers (restriction sites were underlined):

GFP-SOX7_F (HindIII): 5'-CGTAAAGCTTCGATGGCTTCGCTGCTGGG-3'

GFP-SOX7_R (BamHI):

5'-GATCGGATCCCTATGACACACTGTAGCTGTTGTAGT-3'

To generate SOX7-GFP, primers used were:

SOX7-GFP_F (HindIII): 5'-CGTAAAGCTTATGGCTTCGCTGCTGGGAGC-3'

SOX7-GFP_R (BamHI):

5'-GATCGGATCCCGTGACACACTGTAGCTGTTGTAGT-3'

To generate Cherry-HEY1, the primers used were:

Cherry-HEY1_F (HindIII): 5'-CGTAAAGCTTCGATGAAGCGAGCTCACCCC-3'

Cherry-HEY1_R (BamHI): 5'-GATCGGATCCAAAAGCTCCGATCTCCGTCC-3'

To generate HEY1-Cherry, the primers used were:

HEY1-Cherry_F (XhoI): 5'-GATCCTCGAGATGAAGCGAGCTCACCC-3'

HEY1-Cherry_R (HindIII): 5'-CGTAAAGCTTAAAAGCTCCGATCTCGTCC-3'

Full-length SOX7 was sub-cloned into linearised pEGFP-N1 and pEGFP-C1 (Clontech), respectively, to generate SOX7-GFP and GFP-SOX7. Full-length HEY1 was sub-cloned into linearised pmCherry-N1 and pmCherry-C1 (Clontech) to generate HEY1-Cherry and Cherry-HEY1.

To generate expression constructs for luciferase assay,

Full-length HEY1 was amplified from human cDNA library with primers:

pCDNA HEY1_F (EcoRI): 5'-CGTAGAATTCACCATGAAGCGAGCTCACCCC-3'

pCDNA HEY1_R (XhoI):

R: 5'-GATCCTCGAGTTAAAAGCTCCGATCTCCGTCC-3'

And sub-cloned into linearised pCDNA3.1 (Invitrogen) to generate pCDNA HEY1.

Full-length SOX7 was amplified from human cDNA library with primers:

pCDNA SOX7_F (HindIII):

5'-CGTAAAGCTTGCC ATGGCTTCGCTGCTGGGAGC-3'

pCDNA SOX7_R (BamHI):

5'-GATCGGATCC CTATGACACACTGTAGCTGTTGTAGTACGT-3'

And sub-cloned into linearised pCDNA3.1glomyc to generate pCDNA SOX7.

Luciferase constructs

Human VEGFC promoter (hP) was the pGL3-VEGFC promoter-luc-3.4kbHindIII from Kari Alitalo (Chilov et al, 1997). Mouse *Vegfc*

promoter (mP) was pGL4-VEGFC promoter-luc-370 from Min-Jen Hsu (Huang et al, 2014), sub-cloned into linearised pGL3-basic using primers containing HindIII and XhoI restriction enzyme sites (underlined):

-370 mP_Vegfc_F(XhoI): CTAGCCCGGGCTCGAGTCTTCGGGACGAGTGGAAAC

+1 mP_Vegfc_R(HindIII): CCGGAATGCCAAGCTTTGGTGGATGACCCGGGAG

To generate mouse *Vegfc-152* BC-mP-luc construct, the 3.577 kb mouse *Vegfc-152* BC region (GRCm38/mm10_dna range: Chr8:53925003-53928579) and 371 bp mouse VEGFC promoter (-370/+1) were sub-cloned into the linearised pGL3-basic, with primers (restriction sites were underlined):

Insert 1 (*Vegfc-152* BC)

mVegfc-152 BC-mP-luc_1F (XhoI):

5'-GCGTGCTAGCCCGGGCTCGAGTGTGACTAGTGTTCAAATTCCTT-3'

mVegfc-152 BC/RBC-mP-luc_1R:

5'-GTCCCGAAGACATAGATATTGAGATGCCATCTTTT-3'

Insert 2 (VEGFC promoter -370/+1)

mSoxBC/RBC(Vegfc-370/+1)_2F:

5'-AATATCTATGTCTTCGGGACGAGTGGAAAC-3'

mSoxBC/RBC(Vegfc-370/+1)_2R (HindIII):

5'-CAGTACCGGAATGCCAAGCTTGGTGGATGGACCGGGAG-3'

To generate mouse *Vegfc-152* RBC-mP-luc construct, the 6.244 kb mouse *Vegfc-152* BC region (GRCm38/mm10_dna range: Chr8:53922336-53928579) and 371 bp mouse VEGFC promoter (-370/+1) were sub-cloned into the linearised pGL3-basic, with primers (restriction enzyme sites underlined):

Insert 1 (*Vegfc-152* RBC)

mVegfc-152 RBC-mP-luc_1F:

5'-GCGTGCTAGCCCGGGCTCGACAGAACAGGTAGCAGAGGCTA-3'

mVegfc-152 BC/RBC-mP-luc_1R:

5'-GTCCCGAAGACATAGATATTGAGATGCCATCTTTT-3'

Insert 2 (VEGFC promoter -370/+1)

mSoxBC/RBC(Vegfc-370/+1)_2F:

5'-AATATCTATGTCTTCGGGACGAGTGGAAAC-3'

mSoxBC/RBC(Vegfc-370/+1)_2R:

5'-CAGTACCGGAATGCCAAGCTTGGTGGATGGACCGGGAG-3'

pGL3-basic was linearised with XhoI-HF and HindIII-HF.

To generate human *VEGFC-255* BC-hP-luc construct, the 2.014 kb human *VEGFC-255* BC region (GRCh37/hg19_dna range: chr4:177968343-177970356) was sub-cloned into the KpnI linearised pGL3-VEGFC promoter-luc-3.4kbHindIII plasmid, with primers (restriction sites were underlined):

hVEGFC-255 BC/RBC-hP-luc_F (KpnI):

5'-TTTCTCTATCGATAGGTACCAAAGGGTCAAATCGCACAATGC-3'

hVEGFC-255 BC-hP-luc_R (KpnI):

5'-TCGCGTAAGAGCTCGGTACCCAATTGTGCAAGAAGGAGCTTGAG-3'

To generate human *VEGFC-255* RBC-hP-luc construct, the 6.503 kb human *VEGFC-255* RBC region (GRCh37/hg19_dna range: chr4:177,968,343-177,974,845) was sub-cloned into the KpnI linearised pGL3-VEGFC promoter-luc-3.4kbHindIII plasmid, with primers (restriction sites were underlined):

hVEGFC-255 BC/RBC-hP-luc_F (KpnI):

5'-TTTCTCTATCGATAGGTACCAAAGGGTCAAATCGCACAATGC-3'

hVEGFC-255 RBC-hP-luc_R (KpnI):

5'-TCGCGTAAGAGCTCGGTACCACAGATTCTCCCAAGTCTGATAATG-3'

Mouse *Vegfc-152 BC-mP-luc*, *Vegfc-152 RBC-mP-luc*, human *VEGFC-255 BC-hP-luc*, and *VEGFC-255 RBC-hP-luc* constructs were all generated using In-Fusion[®] HD cloning (Takara Bio). Fidelity of the inserts was confirmed with sequencing analysis, with primers:

LucNrev: 5'-CCTTATGCAGTTGCTCTCC-3'

RV_Primer3: 5'-CTAGCAAATAGGCTGTCCC-3'

Luciferase reporter assay

HeLa cells were seeded in triplicate wells per condition in a 24-well plate at 9×10^4 cells/well. Culture media was refreshed prior to transfection with 25 ng pRL-TK (Renilla vector purchased from Promega), 250 ng Firefly luciferase plasmids (pGL3-VEGFC promoter-luc-3.4kbHindIII (hP), pGL3-VEGFC promoter-luc-370 (mP), *Vegfc-152 BC-mP-luc*, *Vegfc-152 RBC-mP-luc*, *VEGFC-255 BC-hP-luc* or *VEGFC-255 RBC-hP-luc*), 12.5 ng of pCDNA3.1 HEY1 (or the empty vector, pCDNA3.1), or 12.5 ng of pCDNA-SOX7 (or the empty vector, pCDNA3.1 Glomyc) as indicated in figure legends for 24 h, using X-tremeGENE9 DNA transfection reagent according to the manufacturer's instructions. Cells were washed twice in PBS and harvested using the dual-luciferase assay reporter system, according to the manufacturer's instructions. To control for transfection efficiency, firefly luciferase activity was determined and normalized to Renilla luciferase activity. Background effects of expression plasmids on pGL3-basic were deducted in all analyses. Readings were then made relative to the human Firefly empty vector-transfected condition, which was set to 1.

Chromatin immunoprecipitation (ChIP) sequencing and library preparations

Briefly, *Sox7-V5* embryos were harvested in ice-cold PBS, pooled, minced, and digested in 0.05% trypsin/EDTA (Invitrogen) at 37°C for 10 min with constant shaking (5 min for E9.5). Solutions were passed through 21- and 23-gauge needles (5–6 times) to isolate single cells, and cell suspensions were next treated with 1% formaldehyde (for DNA-protein cross-linking) in buffer containing 50 mM Hepes-KOH, 0.1 mM NaCl, 1 mM EDTA, 0.5 mM EGTA for 10 min with constant agitation at room temperature. Subsequently, cell suspensions were quenched with 1 mM glycine pH 7.5 for 5 min at room temperature, washed in ice-cold PBS/10% FBS, and finally rinsed in ice-cold PBS. The resultant cell pellet from each

litter was snapped frozen on dry ice before storage at -80°C . All steps were carried out on ice unless specified. Cell pellets were next thawed on ice, and pellets across different litters from a similar developmental stage were pooled together before cell lysis. After sonication, 50 μL from each sonication sample was kept aside (this is the input DNA control) before the immunoprecipitation step using 10 μg V5 monoclonal antibody (R960CUS, Invitrogen). The subsequent steps were carried out as detailed in the published protocol (Schmidt *et al*, 2009). Following immunoprecipitation, DNA amplification was performed on both the IP sample and input DNA control using TruSeq ChIPseq kit (Illumina, IP-202-1012) with 0.5 μM of the universal forward and reverse PCR primer containing the index sequence of choice in 50 μL 1 \times NEB Next High-Fidelity PCR Master Mix (New England Biolabs, M0541). The number of PCR cycles ranged from 13 to 18, depending on the ChIP efficiency. The PCR product was purified using AMPure beads (1.8 volume) and eluted in 20 μL of resuspension buffer (Tris-Acetate 10 mM pH 8). The library was quantified using the KAPA library quantification kit for Illumina sequencing platforms (KAPA Biosystems, KK4824) and 50 bp single-end reads were sequenced on a HiSeq2500 following the manufacturer's protocol.

ChIP-sequencing peak calling, genome annotation, and visualization

After sequencing, FASTA files were uploaded onto Galaxy Australia (Afgan *et al*, 2015). Quality control was performed on the sequence reads using FastQC (Galaxy version 0.53) (Available from <https://www.bioinformatics.babraham.ac.uk/projects/fastqc/>). Reads were filtered and trimmed by Trimmomatic (Galaxy version 0.32.2) (Bolger *et al*, 2014), before alignment to the latest mouse reference genome Genome Reference Consortium (GRC) m38/mm10 (released in Dec 2011) using Bowtie2 (Galaxy version 2.2.6.2) (Langmead & Salzberg, 2012). Repeated sequences were filtered and unique sequences were called using MACS version 2.1.0 (Zhang *et al*, 2008). Potential binding regions of SOX7 (or peaks) were called using each corresponding input DNA as reference, with a false discovery rate (FDR) of 0.01. The SOX7-V5 ChIP-Seq shows an expected percentage of uniquely mapped reads for a mouse ChIP-seq (Bailey *et al*, 2013), with > 70% unique reads aligned to the reference genome. Only the unique reads were considered for peak calling.

In both SOX7 HUVECs and SOX7-V5 Chip-Seq, binding regions (peaks) were visualized using either UCSC Genome Browser (available at <https://genome.ucsc.edu/>) or Integrative Genomics Viewer IGV version 2.3.92 (Robinson *et al*, 2011). Peaks to Genes (top 2k only, ranked by their estimated enrichment folds as depicted in the interval files after peak calling) were annotated by Gene Regions Enrichment of Annotations (GREAT) version 3.0.0 with GRC37/hg19 for human and GRCm38/mm10 for mouse dataset (McLean *et al*, 2010). Distance of binding regions in relation to the gene transcription start sites (TSS) regions was used as a proxy for the likelihood of transcription regulation.

De novo and local enrichment motif analysis

Motif discovery was performed on the top 2k peaks from E9.5 and E10.5. Sequences in FASTA format 500 bp around the peak center were created using the "Extract genomic DNA" tool from Galaxy

(version 2.2.3) or “GetFastaBed” from Galaxy (version 20.01). The fetched sequences were subsequently piped into Multiple EM for Motif Elicitation (MEME)-ChIP version 5.1.1, using the default settings with the following changes: (i) “JASPAR Vertebrates and UniPROBE Mouse” were used as the input motif (ii) Under the MEME options, the expected motif site distribution was changed to “any number of repetitions,” and the minimum motif width was changed to 4bp (iii) Under Central Motif Enrichment Analysis (CentriMo), the local mode has been enabled to find uncentered regions (Machanic & Bailey, 2011). Spaced Motif (SpaMo) analysis tool was used to identify enriched spacing between a primary motif and each identified secondary motifs. To identify the total occurrences of the *de novo* motifs discovered by MEME, the Find Individual Motif Occurrences (FIMO) tool was used (Bailey et al, 2009, 2015). All described tools are available at MEME-suite (<http://meme-suite.org/tools/meme-chip>).

Pathway enrichment analysis

Genes associated with the top 2k peaks from SOX7 HUVEC ChIP-Seq (E-MTAB-4480) were used for pathway enrichment search using the GREAT v1.8 Molecular Signatures Database (MSigDB) pathway analysis (Subramanian et al, 2005). Only the top 5 most enriched pathways associated with the gene set were reported.

Histone mark and chromatin state SOX7 ChIP-Seq analysis

Bed files with the top 2k of SOX7 HUVEC ChIP-Seq peaks were uploaded onto the EpiExplorer online tool. Histone states and chromatin state segmentation were analyzed using the tool function. Regions associated with at least 50% of the chromatin state/histone markers were then exported into Venny 2.1.0 to generate Venn diagrams. For SOX7-V5 ChIP-Seq, the GRCh38/mm10 version of the top 2k peaks from E9.5 and E10.5 was liftOver to mm9 using the UCSC Genome Browser. These converted tracks were then uploaded on the EpiExplorer online tool to be overlapped with histone markers from the ENCODE database. Chromatin state segmentation analysis is not available for mouse data. Corresponding regions associated with at least 50% overlapping with each histone marks were next exported into Venny 2.1.0 to generate Venn diagrams.

Antibodies

For immunostaining, primary antibodies were rat anti-EMCN (1:300, sc-53941, Santa Cruz), goat anti-NRP2 (1:300, AF567, R&D System), goat anti-SOX7 (1:300, AF2766, R&D System), goat anti-SOX17 (1:300, AF1924, R&D System), rabbit anti-PROX1 (1:300, 11-002, Abcam), rabbit anti-ERG (1:300, AB92513, Abcam), rat anti-phospho-histone H3 (1:500; H9908, Sigma Aldrich), rabbit anti-V5 (1:200, AB3792, Merck), chicken anti-beta galactosidase (1:200, AB9361, Abcam), and DAPI (1:1,000, D9542, Sigma Aldrich).

Secondary antibodies were goat anti-chicken IgG Alexa 488 (A11039), donkey anti-goat IgG Alexa 647 (A21447), donkey anti-rat IgG Alexa 488 (A21208), donkey anti-rabbit Alexa 594 (A21207), donkey anti-rabbit IgG Alexa 647 (A31573), donkey, and anti-goat IgG Alexa 594 (A11058), goat anti-rat IgG Alexa 594 (A11007), and goat anti-rat IgG Alexa 647 (A21247). Secondary antibodies were sourced from Invitrogen and used at 1:300 unless specified otherwise.

For co-immunoprecipitation and western blotting, primary antibodies were: Living Colors Ds-red rabbit antibody (632496, Clontech), rabbit anti-tubulin (T3526, Sigma Aldrich), and mouse anti-GFP (3E6) (A-11120, Thermo-Scientific). Secondary antibodies were goat anti-rabbit IgG HRP (65-6120) and goat anti-mouse IgG HRP (A10551). Secondary antibodies were sourced from Invitrogen, and all antibodies were used at 1:1,000.

For the cell-sorting experiment, antibodies were Alexa 488 conjugated rat anti-CD31 (1:200, 563607, BD Pharmingen) and PE/Cy5 rat anti-CD45 (1:1,000, 103109, BioLegend); live/dead cells were detected by DAPI (1:1,000, D9542, Sigma Aldrich).

CDNA synthesis and real-time PCR

First-strand cDNA was synthesized from 1,500 ng purified RNA using High-Capacity cDNA Reverse Transcription Kit (Life technologies). qPCR was performed and analyzed as described by Chiang et al, 2017. To quantify the transcript level of target genes, primers used were:

mSox7_F: 5'-GCGGAGCTCAGCAAGATG-3'
 mSox7_R: 5'-GGGTCTCTCTGGGACAGTG-3'
 mSox17_F: 5'-CACAAACGCAGAGCTAAGCAA-3'
 mSox17_R: 5'-CGCTTCTCTGCCAAGGTC-3'
 mSox18_F: 5'-ACTGGCGCAACAAAATCC-3'
 mSox18_R: 5'-CTTCTCCGCCGTGTTTCAG-3'
 mVegfr3_F: 5'-GGTTCCTGATGGGCAAAGG-3'
 mVegfr3_R: 5'-TCAGTGGGCTCAGCCATAGG-3'
 mHey1_F: 5'-CATGAAGAGAGCTCACCCAGA-3'
 mHey1_R: 5'-CGCCGAACCTCAAGTTTCC-3'
 mVegfr2_F: 5'-CAGTGGTACTGGCAGTAGAAG-3'
 mVegfr2_R: 5'-ACAAGCATACGGGCTTGT-3'
 mDll4_F: 5'-AGGTGCCACTTCCGTTACAC-3'
 mDll4_R: 5'-GGGAGAGCAAATGGCTGATA-3'
 mNotch1_F: 5'-CTGGACCCCATGGACATC-3'
 mNotch1_R: 5'-AGGATGACTGCACACATTGC-3'
 mPecam_F: 5'-CGGTGTTCCAGCGAGATCC-3'
 mPecam_R: 5'-ACTCGACAGGATGGAAATCAC-3'
 mCdh5_F: 5'-GTTCAAGTTTGCCTGAAGAA-3'
 mCdh5_R: 5'-GTGATGTTGGCGGTGTTGT-3'

mVegfc primers sequenced were from (Hominick et al, 2018).

hSOX7_F: 5'-AGCTGTCCGATGGACAATCG-3'
 hSOX7_R: 5'-CCACGACTTCCCAGCATCT-3'
 hVEGFR3_F: 5'-ATAGACAAGAAAGCGGCTTCA-3'
 hVEGFR3_R: 5'-CCTCCCTGGGAGTCAGG-3'
 hVEGFR2_F: 5'-GAACATTTGGGAAATCTCTTGC-3'
 hVEGFR2_R: 5'-CGGAAGAACAATGTAGTCTTGC-3'
 hGAPDH_F: 5'-CCCCGGTTTCTATAAAATTGAGC-3'
 hGAPDH_R: 5'-CACCTTCCCATGGTGTCT-3'
 hHEY1_F: 5'-CATACGGCAGGAGGGAAAG-3'
 hHEY1_R: 5'-GCATCTAGTCTTCAATGATGCT-3'
 hVEGFC_F: 5'-CACTACCACAGTGTCCAGGCA-3'
 hVEGFC_R: 5'-GTCATCTCCAGCATCCGAGG-3'
 hVEGFA_F: 5'-AGGGAAGGGGCAAAAACGA-3'
 hVEGFA_R: 5'-CCTCGGCTGTGCATCTGC-3'
 hPROX1_F: 5'-TCACCTTATTCGGGAAGTGC-3'
 hPROX1_R: 5'-GAGCTGGGATAACGGGTATAAA-3'
 hGAPDH_F: 5'-CCCCGGTTTCTATAAAATTGAGC-3'

hGAPDH_R: 5'-CACCTTCCCCATGGTGTCT-3'
 hHPRT_F: 5'-AATGACCAGTCAACAGGGGACA-3'
 hHPRT_R: 5'-TACTGCCTGACCAAGGAAAGCA-3

Quantification and data analysis

To quantify the proportion of SOX7-positive cells in Fig 1A, SOX7⁺ cells were calculated manually using ImageJ and subsequently divided by ERG⁺ endothelial cells in the entire section. Fig 1D–J were quantified within 2,100 μm from both sides of the midline. LEC front distance to the midline (Fig 1D) was an average of 10 random measurements taken from the midline to the nearest leading lymphatic sprouts. For vessel width (Fig 1F), three locations within 200 μm from the sprouting end of each lymphatic leading vessel were measured. Vessel width was taken from the average of seven representative lymphatic leading vessels in each embryo. PROX1⁺ nuclei in Fig 1H were an average of PROX1⁺ number quantified from the 7 representative lymphatic leading vessels in Fig 1F (200 μm from the sprouting end). For Fig 1J disconnected vessels (> 100 μm) or lymphatic endothelial cell (LEC) clusters (< 100 μm) are defined as PROX1⁺ NRP2⁺ cell population that is isolated from the lymphatic network. Only the PROX1⁺ nuclei in a single LEC cluster were quantified and shown in Fig 1I.

To quantify the % of PROX1⁺ cells within the indicated region in the cardinal veins (CVs) (Fig 5B), CVs were divided into a 12-section pie chart. Region nearest to the dorsal aorta was designated as 0/360°. Within each region, the number of PROX1⁺ LEC progenitors and EMCN⁺ DAPI⁺ endothelial cells were quantified. Each region from Fig 5A–C was the average of 20 and 17 vibratome sections from sibling controls (*n* = 5) and *Sox7*^{IECKO} mutants (*n* = 4), respectively. Only sections from middle to lower thoracic regions were included for analysis. Data were then plotted in a rose diagram using Visual Paradigm online Diagrams.

To quantify the number of PROX1⁺ LECs or LEC clusters associated with EMCN⁺ BV (Fig 5D and E), confocal images were taken randomly from each skin quadrants: left/ right cervical, thoraco-cervical, and thoraco-lumbar regions. To effectively quantify the PROX1⁺ LECs associated with LV, EMCN⁺ surface was created by the “surface” function in Imaris, which was then masked for PROX1⁺ cells. Then, PROX1⁺ cells were counted manually by carefully going through each image slices and scrutinized also in 3D projection. PROX1⁺ cells that belong to the greater lymphatic networks and isolated from BV were excluded. PROX1⁺ cell types were categorized according to Appendix Fig S10A and B. Where a PROX1⁺ cell or cluster appears to be associated with BV, a confocal image at a higher resolution (X40–X63) would be taken for further confirmation. Total PROX1⁺ cells were finally normalized to the total BV surface area analyzed.

Vessel front density (Fig EV2B) was quantified from EMCN⁺ blood vessels 500 μm from the midline (700 × 3,072 μm) using the “surface” function in Imaris. The number of H3⁺ ERG⁺ proliferative endothelial cells and total EGR⁺ endothelial cells from the same region were quantified with the “spot” function in Imaris.

Figure EV2D–H were quantified from a similar area of skins (3,500 × 2,000 μm), using the “surface” and “spots” function in Imaris. Green BV was the green area that co-localized with EMCN⁺ surface. Total blood vessel (BV) surface density was a surface rendering of the EMCN⁺ vessel. Percentage of Cre recombination in

BV was therefore green BV density/total BV density (Fig EV2D). Total lymphatic endothelial cells (LECs) were quantified by spots rendering PROX1⁺ nuclei. Total green LECs were determined by spots rendering of green cells, which were also PROX1⁺. The percentage of Cre recombination in the lymphatic vessel (LV) was therefore Green LECs/Total LECs (Fig EV2E). Branching points and lymphatic vessel width were quantified as described in Fig 1E and F (Fig EV2F and G). BV blood density was total EMCN⁺ BV surface (Fig EV2H).

Data availability

The ChIP-Seq data are available in the ArrayExpress database at EMBL-EBI (<https://www.ebi.ac.uk/fg/annotare/>) with accession number E-MTAB-12320 (<https://www.ebi.ac.uk/biostudies/arrayexpress/studies/E-MTAB-12320>).

Expanded View for this article is available online.

Acknowledgements

The authors would like to thank Dr Ming-Jen Hsu for the kind gift of the mouse luciferase reporter construct, pGL4-VEGFC promoter-luc-370, Dr. Dmitri Chilov for help in obtaining the human VEGFC promoter constructs, Dr Emma Gordon for the *mT/mG* mice, and Dr Luciano Martelotto and Dr Yen Tran for nuclei isolation protocol in single-nuclei RNA-Seq. We thank Dr Carol Wicking for scientific comments and advice on the editing of the manuscript. This research was supported by the National Health and Medical Research Council (NHMRC) grant and fellowship (APP1107643, APP116400, and AP1111169), and ARC grant (DP200100250) to MF. The authors would like to acknowledge the technical and scientific assistance of Sydney Microscopy and Microanalysis, the University of Sydney node of Microscopy Australia, ACRF Cancer Biology Imaging Facility at the Institute for Molecular Bioscience, and the Flow Cytometry Facility at Queensland Brain Institute. Synopsis Figure and Fig 6C are created with BioRender.com. Open access publishing facilitated by The University of Sydney, as part of the Wiley - The University of Sydney agreement via the Council of Australian University Librarians.

Author contributions

Mathias Francois: Conceptualization; formal analysis; supervision; funding acquisition; writing—original draft; project administration; writing—review and editing. **Ivy K N Chiang:** Conceptualization; formal analysis; supervision; validation; investigation; visualization; methodology; writing—original draft; project administration; writing—review and editing. **Matthew S Graus:** Formal analysis; investigation; methodology. **Nils Kirschnick:** Investigation. **Tara Davidson:** Investigation. **Winnie Luu:** Formal analysis; investigation. **Richard Harwood:** Formal analysis; methodology. **Keyi Jiang:** Formal analysis. **Bitong Li:** Investigation. **Yew Yan Wong:** Investigation. **Mehdi Moustaqil:** Formal analysis; investigation. **Emmanuelle Lesieur:** Investigation. **Rena Skoczylas:** Investigation. **Valerie Kouskoff:** Supervision. **Jan Kazenwadel:** Investigation. **Luis Arriola-Martinez:** Investigation. **Emma Sierecki:** Supervision. **Yann Gambin:** Supervision. **Kari K Alitalo:** Resources; supervision; writing—review and editing. **Friedmann Kiefer:** Supervision; writing—review and editing. **Natasha L Harvey:** Supervision.

Disclosure and competing interests statement

The authors declare that they have no conflict of interest.

References

- Afgan E, Sloggett C, Goonasekera N, Makunin I, Benson D, Crowe M, Gladman S, Kowsar Y, Pheasant M, Horst R et al (2015) Genomics virtual laboratory: a practical bioinformatics workbench for the cloud. *PLoS One* 10: e0140829
- Alquicira-Hernandez J, Powell JE (2021) Nebulosa recovers single-cell gene expression signals by kernel density estimation. *Bioinformatics* <https://doi.org/10.1093/bioinformatics/btab003>
- Bailey TL, Boden M, Buske FA, Frith M, Grant CE, Clementi L, Ren J, Li WW, Noble WS (2009) MEME Suite: tools for motif discovery and searching. *Nucleic Acids Res* 37: W202–W208
- Bailey T, Krajewski P, Ladunga I, Lefebvre C, Li Q, Liu T, Madrigal P, Taslim C, Zhang J (2013) Practical guidelines for the comprehensive analysis of ChIP-seq data. *PLoS Comput Biol* 9: e1003326
- Bailey TL, Johnson J, Grant CE, Noble WS (2015) The MEME Suite. *Nucleic Acids Res* 43: W39–W49
- Benjamini Y, Hochberg Y (1995) Controlling the false discovery rate: a practical and powerful approach to multiple testing. *J Roy Statist Soc* 57: 289–300
- Bolger AM, Lohse M, Usadel B (2014) Trimmomatic: a flexible trimmer for Illumina sequence data. *Bioinformatics* 30: 2114–2120
- Bowles J, Secker G, Nguyen C, Kazenwadel J, Truong V, Frampton E, Curtis C, Skoczylas R, Davidson TL, Miura N et al (2014) Control of retinoid levels by CYP26B1 is important for lymphatic vascular development in the mouse embryo. *Dev Biol* 386: 25–33
- Brash JT, Bolton RL, Rashbrook VS, Denti L, Kubota Y, Ruhrberg C (2020) Tamoxifen-Activated CreERT Impairs Retinal Angiogenesis Independently of Gene Deletion. *Circ Res* 127: 849–850
- Bussmann J, Bos FL, Urasaki A, Kawakami K, Duckers HJ, Schulte-Merker S (2010) Arteries provide essential guidance cues for lymphatic endothelial cells in the zebrafish trunk. *Development* 137: 2653
- Butler A, Hoffman P, Smibert P, Papalexi E, Satija R (2018) Integrating single-cell transcriptomic data across different conditions, technologies, and species. *Nat Biotechnol* 36: 411–420
- Cahill TJ, Sun X, Ravaut C, Villa del Campo C, Klaurakis K, Lupu I-E, Lord AM, Browne C, Jacobsen SEW, Greaves DR et al (2021) Tissue-resident macrophages regulate lymphatic vessel growth and patterning in the developing heart. *Development* 148: dev194563
- Cao Y, Linden P, Farnebo J, Cao R, Eriksson A, Kumar V, Qi JH, Claesson-Welsh L, Alitalo K (1998) Vascular endothelial growth factor C induces angiogenesis in vivo. *Proc Natl Acad Sci USA* 95: 14389–14394
- Cha YR, Fujita M, Butler M, Isogai S, Kochhan E, Siekmann AF, Weinstein BM (2012) Chemokine signaling directs trunk lymphatic network formation along the preexisting blood vasculature. *Dev Cell* 22: 824–836
- Chen HI, Poduri A, Numi H, Kivela R, Saharinen P, McKay AS, Raftrey B, Churko J, Tian X, Zhou B et al (2014) VEGF-C and aortic cardiomyocytes guide coronary artery stem development. *J Clin Invest* 124: 4899–4914
- Chew LJ, Gallo V (2009) The Yin and Yang of Sox proteins: Activation and repression in development and disease. *J Neurosci Res* 87: 3277–3287
- Chiang IK-N, Fritzsche M, Pichol-Thieuvend C, Neal A, Holmes K, Lagendijk A, Overman J, Angelo D, Omini A, Hermkens D et al (2017) SoxF factors induce Notch1 expression via direct transcriptional regulation during early arterial development. *Development* 144: 2629–2639
- Chilov D, Kukk E, Taira S, Jeltsch M, Kaukonen J, Palotie A, Joukov V, Alitalo K (1997) Genomic organization of human and mouse genes for vascular endothelial growth factor C. *J Biol Chem* 272: 25176–25183
- Cohen B, Tempelhof H, Raz T, Oren R, Nicenboim J, Bochner F, Even R, Jelinski A, Eilam R, Ben-Dor S et al (2020) BACH family members regulate angiogenesis and lymphangiogenesis by modulating VEGFC expression. *Life Sci Alliance* 3: e202000666
- Corada M, Orsenigo F, Morini MF, Pitulescu ME, Bhat G, Nyqvist D, Breviario F, Conti V, Briot A, Iruela-Arispe ML et al (2013) Sox17 is indispensable for acquisition and maintenance of arterial identity. *Nat Commun* 4: 2609
- Costa G, Mazan A, Gandillet A, Pearson S, Lacaud G, Kouskoff V (2012) SOX7 regulates the expression of VE-cadherin in the haemogenic endothelium at the onset of haematopoietic development. *Development* 139: 1587–1598
- Cruz-Molina S, Respuela P, Tebartz C, Kolovos P, Nikolic M, Fueyo R, van Ijcken WFJ, Grosveld F, Frommolt P, Bazzi H et al (2017) PRC2 facilitates the regulatory topology required for poised enhancer function during pluripotent stem cell differentiation. *Cell Stem Cell* 20: 689–705.e689
- Cuddapah S, Jothi R, Schones DE, Roh TY, Cui K, Zhao K (2009) Global analysis of the insulator binding protein CTCF in chromatin barrier regions reveals demarcation of active and repressive domains. *Genome Res* 19: 24–32
- Duong T, Koltowska K, Pichol-Thieuvend C, Le Guen L, Fontaine F, Smith KA, Truong V, Skoczylas R, Stacker SA, Achen MG et al (2013) VEGFD regulates blood vascular development by modulating SOX18 activity. *Blood* 123: 1102–1112
- Fan R, He H, Yao W, Zhu Y, Zhou X, Gui M, Lu J, Xi H, Deng Z, Fan M (2018) SOX7 suppresses Wnt signaling by disrupting β -catenin/BCL9 interaction. *DNA Cell Biol* 37: 126–132
- Filippova GN, Fagerlie S, Klenova EM, Myers C, Dehner Y, Goodwin G, Neiman PE, Collins SJ, Lobanenko VV (1996) An exceptionally conserved transcriptional repressor, CTCF, employs different combinations of zinc fingers to bind diverged promoter sequences of avian and mammalian c-myc oncogenes. *Mol Cell Biol* 16: 2802–2813
- Fischer A, Klattig J, Kneitz B, Diez H, Maier M, Holtmann B, Englert C, Gessler M (2005) Hey basic helix-loop-helix transcription factors are repressors of GATA4 and GATA6 and restrict expression of the GATA target gene ANF in fetal hearts. *Mol Cell Biol* 25: 8960–8970
- François M, Caprini A, Hosking B, Orsenigo F, Wilhelm D, Browne C, Paavonen K, Karnezis T, Shayan R, Downes M et al (2008) Sox18 induces development of the lymphatic vasculature in mice. *Nature* 456: 643–647
- François M, Koopman P, Beltrame M (2010) SoxF genes: key players in the development of the cardio-vascular system. *Int J Biochem Cell Biol* 42: 445–448
- Futaki S, Hayashi Y, Emoto T, Weber CN, Sekiguchi K (2004) Sox7 plays crucial roles in parietal endoderm differentiation in F9 embryonal carcinoma cells through regulating Gata-4 and Gata-6 expression. *Mol Cell Biol* 24: 10492–10503
- Gandillet A, Serrano AG, Pearson S, Lie-A-Ling M, Lacaud G, Kouskoff V (2009) Sox7-sustained expression alters the balance between proliferation and differentiation of hematopoietic progenitors at the onset of blood specification. *Blood* 114: 4813–4822
- Gauvrit S, Villaseñor A, Strlic B, Kitchen P, Collins MM, Marín-Juez R, Guenther S, Maischein HM, Fukuda N, Canham MA et al (2018) HHX is a transcriptional regulator of the VEGFC/FLT4/PROX1 signaling axis during vascular development. *Nat Commun* 9: 2704
- Gordon EJ, Rao S, Pollard JW, Nutt SL, Lang RA, Harvey NL (2010) Macrophages define dermal lymphatic vessel calibre during development by regulating lymphatic endothelial cell proliferation. *Development* 137: 3899–3910

- Guo L, Zhong D, Lau S, Liu X, Dong X-Y, Sun X, Yang VW, Vertino PM, Moreno CS, Varma V *et al* (2008) Sox7 is an independent checkpoint for β -Catenin function in prostate and colon epithelial cells. *Mol Cancer Res* 6: 1421–1430
- Hermkens DMA, van Impel A, Urasaki A, Bussmann J, Duckers HJ, Schulte-Merker S (2015) Sox7 controls arterial specification in conjunction with *hey2* and *efnb2* function. *Development* 142: 1695–1704
- Hogan BM, Herpers R, Witte M, Heloterä H, Alitalo K, Duckers HJ, Schulte-Merker S (2009) Vegfc/Flt4 signalling is suppressed by Dll4 in developing zebrafish intersegmental arteries. *Development* 136: 4001
- Hominick D, Silva A, Khurana N, Liu Y, Dechow PC, Feng JQ, Pytowski B, Rutkowski JM, Alitalo K, Dellinger MT (2018) VEGF-C promotes the development of lymphatics in bone and bone loss. *eLife* 7: e34323
- Hosking BM, Wang SCM, Chen SL, Penning S, Koopman P, Muscat GEO (2001) SOX18 directly interacts with MEF2C in endothelial cells. *Biochem Biophys Res Commun* 287: 493–500
- Hosking BM, Wang SCM, Downes M, Koopman P, Muscat GEO (2004) The VCAM-1 gene that encodes the vascular cell adhesion molecule is a target of the Sry-related high mobility group box gene, Sox18. *J Biol Chem* 279: 5314–5322
- Huang Y-H, Yang H-Y, Hsu Y-F, Chiu P-T, Ou G, Hsu M-J (2014) Src contributes to IL6-induced vascular endothelial growth factor-C expression in lymphatic endothelial cells. *Angiogenesis* 17: 407–418
- Ip YT (1995) Transcriptional regulation. Converting an activator into a repressor. *Curr Biol* 5: 1–3
- Kampmeier OF (1969) *Evolution and comparative morphology of the lymphatic system*. Springfield, IL: Thomas
- Karkkainen MJ, Haiko P, Sainio K, Partanen J, Taipale J, Petrova TV, Jeltsch M, Jackson DG, Talikka M, Rauvala H *et al* (2004) Vascular endothelial growth factor C is required for sprouting of the first lymphatic vessels from embryonic veins. *Nat Immunol* 5: 74–80
- Kazenwadel J, Michael MZ, Harvey NL (2010) Prox1 expression is negatively regulated by miR-181 in endothelial cells. *Blood* 116: 2395–2401
- Kazenwadel J, Secker GA, Betterman KL, Harvey NL (2012) In vitro assays using primary embryonic mouse lymphatic endothelial cells uncover key roles for FGFR1 signalling in lymphangiogenesis. *PLoS One* 7: e40497
- Kim K, Kim I-K, Yang JM, Lee E, Koh BI, Song S, Park J, Lee S, Choi C, Kim JW *et al* (2016) SOXF transcription factors are positive feedback regulators of VEGF signaling. *Circ Res* 121: 839–852
- Langmead B, Salzberg SL (2012) Fast gapped-read alignment with Bowtie 2. *Nat Methods* 9: 357–359
- Lilly AJ, Costa G, Largeot A, Fadlullah MZH, Lie-A-Ling M, Lacaud G, Kouskoff V (2016) Interplay between SOX7 and RUNX1 regulates hemogenic endothelial fate in the yolk sac. *Development* 143: 4341
- Lilly AJ, Mazan A, Scott DA, Lacaud G, Kouskoff V (2017) SOX7 expression is critically required in FLK1-expressing cells for vasculogenesis and angiogenesis during mouse embryonic development. *Mech Dev* 146: 31–41
- Liu X, Uemura A, Fukushima Y, Yoshida Y, Hirashima M (2016) Semaphorin 3G provides a repulsive guidance cue to lymphatic endothelial cells via Neuropilin-2/PlexinD1. *Cell Rep* 17: 2299–2311
- Lohela M, Heloterä H, Haiko P, Dumont DJ, Alitalo K (2008) Transgenic induction of vascular endothelial growth factor-C is strongly angiogenic in mouse embryos but leads to persistent lymphatic hyperplasia in adult tissues. *Am J Pathol* 173: 1891–1901
- Machanic P, Bailey TL (2011) MEME-ChIP: motif analysis of large DNA datasets. *Bioinformatics* 27: 1696–1697
- Mäkinen T, Veikkola T, Mustjoki S, Karpanen T, Catimel B, Nice EC, Wise L, Mercer A, Kowalski H, Kerjaschki D *et al* (2001) Isolated lymphatic endothelial cells transduce growth, survival and migratory signals via the VEGF-C/D receptor VEGFR-3. *EMBO J* 20: 4762–4773
- Martinez-Corral I, Ulvmar M, Stanczuk L, Tatin F, Kizhatil K, John SWM, Alitalo K, Ortega S, Makinen T (2015) Non-venous origin of dermal lymphatic vasculature. *Circ Res* 116: 1649–1654
- Maruyama K, Naemura K, Arima Y, Uchijima Y, Nagao H, Yoshihara K, Singh MK, Uemura A, Matsuzaki F, Yoshida Y *et al* (2021) Semaphorin3E-PlexinD1 signaling in coronary artery and lymphatic vessel development with clinical implications in myocardial recovery. *iScience* 24: 102305
- McLean CY, Bristor D, Hiller M, Clarke SL, Schaar BT, Lowe CB, Wenger AM, Bejerano G (2010) GREAT improves functional interpretation of cis-regulatory regions. *Nat Biotechnol* 28: 495–501
- Mohammed H, D'Santos C, Serandour Aurelien A, Ali HR, Brown Gordon D, Atkins A, Rueda Oscar M, Holmes Kelly A, Theodorou V, Robinson Jessica LL *et al* (2013) Endogenous purification reveals GREB1 as a key estrogen receptor regulatory factor. *Cell Rep* 3: 342–349
- Moustaqil M, Fontaine F, Overman J, McCann A, Bailey TL, Rudolffi Soto P, Bhumkar A, Giles N, Hunter DJB, Gambin Y *et al* (2018) Homodimerization regulates an endothelial specific signature of the SOX18 transcription factor. *Nucleic Acids Res* 46: 11381–11395
- Murakami A, Shen H, Ishida S, Dickson C (2004) SOX7 and GATA-4 are competitive activators of Fgf-3 transcription. *J Biol Chem* 279: 28564–28573
- Murtomaki A, Uh MK, Choi YK, Kitajewski C, Borisenko V, Kitajewski J, Shawber CJ (2013) Notch1 functions as a negative regulator of lymphatic endothelial cell differentiation in the venous endothelium. *Development* 140: 2365–2376
- Muzumdar MD, Tasic B, Miyamichi K, Li L, Luo L (2007) A global double-fluorescent Cre reporter mouse. *Genesis* 45: 593–605
- Nakagawa O, McFadden DG, Nakagawa M, Yanagisawa H, Hu T, Srivastava D, Olson EN (2000) Members of the HRT family of basic helix-loop-helix proteins act as transcriptional repressors downstream of Notch signaling. *Proc Natl Acad Sci USA* 97: 13655–13660
- Ngan CY, Wong CH, Tjong H, Wang W, Goldfeder RL, Choi C, He H, Gong L, Lin J, Urban B *et al* (2020) Chromatin interaction analyses elucidate the roles of PRC2-bound silencers in mouse development. *Nat Genet* 52: 264–272
- Niimi T, Hayashi Y, Futaki S, Sekiguchi K (2004) SOX7 and SOX17 regulate the parietal endoderm-specific enhancer activity of mouse laminin α 1 gene. *J Biol Chem* 279: 38055–38061
- Overman J, Fontaine F, Moustaqil M, Mittal D, Sierrecki E, Sacilotto N, Zuegg J, Robertson AAB, Holmes K, Salim AA *et al* (2017) Pharmacological targeting of the transcription factor SOX18 delays breast cancer in mice. *eLife* 6: e21221
- Pang B, Snyder MP (2020) Systematic identification of silencers in human cells. *Nat Genet* 52: 254–263
- Pichol-Thievend C, Betterman KL, Liu X, Ma W, Skoczylas R, Lesieur E, Bos FL, Schulte D, Schulte-Merker S, Hogan BM *et al* (2018) A blood capillary plexus-derived population of progenitor cells contributes to genesis of the dermal lymphatic vasculature during embryonic development. *Development* 145: dev160184
- Polanco JC, Wilhelm D, Davidson T-L, Knight D, Koopman P (2010) Sox10 gain-of-function causes XX sex reversal in mice: implications for human 22q-linked disorders of sex development. *Hum Mol Genet* 19: 506–516
- Rauniyar K, Jha SK, Jeltsch M (2018) Biology of Vascular Endothelial Growth Factor C in the Morphogenesis of Lymphatic Vessels. *Front Bioeng Biotechnol* 6: 7

- Robinson JT, Thorvaldsdottir H, Winckler W, Guttman M, Lander ES, Getz G, Mesirov JP (2011) Integrative genomics viewer. *Nat Biotechnol* 29: 24–26
- Sacilotto N, Monteiro R, Fritzsche M, Becker PW, Sanchez-del-Campo L, Liu K, Pinheiro P, Ratnayaka I, Davies B, Goding CR et al (2013) Analysis of Dll4 regulation reveals a combinatorial role for Sox and Notch in arterial development. *Proc Natl Acad Sci USA* 110: 11893–11898
- Schmidt D, Wilson MD, Spyrou C, Brown GD, Hadfield J, Odom DT (2009) ChIP-seq: Using high-throughput sequencing to discover protein–DNA interactions. *Methods* 48: 240–248
- Schock EN, LaBonne C (2020) Sorting Sox: diverse roles for Sox transcription factors during neural crest and craniofacial development. *Front Physiol* 11: 606889
- Schuermann A, Helker CS, Herzog W (2015) Metallothionein 2 regulates endothelial cell migration through transcriptional regulation of vegf expression. *Angiogenesis* 18: 463–475
- Sierecki E, Stevers LM, Giles N, Polinkovsky ME, Moustaqil M, Mureev S, Johnston WA, Dahmer-Heath M, Skalamera D, Gonda TJ et al (2014) Rapid mapping of interactions between Human SNX-BAR proteins measured in vitro by AlphaScreen and single-molecule spectroscopy. *Mol Cell Proteomics* 13: 2233–2245
- Srinivasan RS, Dillard ME, Lagutin OV, Lin F-J, Tsai S, Tsai M-J, Samokhvalov IM, Oliver G (2007) Lineage tracing demonstrates the venous origin of the mammalian lymphatic vasculature. *Genes Dev* 21: 2422–2432
- Srinivasan RS, Escobedo N, Yang Y, Interiano A, Dillard ME, Finkelstein D, Mukatira S, Gil HJ, Nurmi H, Alitalo K (2014) The Prox1–Vegfr3 feedback loop maintains the identity and the number of lymphatic endothelial cell progenitors. *Genes Dev* 28: 2175–2187
- Subramanian A, Tamayo P, Mootha VK, Mukherjee S, Ebert BL, Gillette MA, Paulovich A, Pomeroy SL, Golub TR, Lander ES et al (2005) Gene set enrichment analysis: A knowledge-based approach for interpreting genome-wide expression profiles. *Proc Natl Acad Sci USA* 102: 15545
- Tammela T, Zarkada G, Wallgard E, Murtomaki A, Suchting S, Wirzenius M, Waltari M, Hellstrom M, Schomber T, Peltonen R et al (2008) Blocking VEGFR-3 suppresses angiogenic sprouting and vascular network formation. *Nature* 454: 656–660
- del Toro R, Prahst C, Mathivet T, Siegfried G, Kaminker JS, Larrivee B, Breant C, Duarte A, Takakura N, Fukamizu A et al (2010) Identification and functional analysis of endothelial tip cell-enriched genes. *Blood* 116: 4025–4033
- Uchida Y, James JM, Suto F, Mukoyama Y-s (2015) Class 3 semaphorins negatively regulate dermal lymphatic network formation. *Biol Open* 4: 1194
- Uchikawa M, Kamachi Y, Kondoh H (1999) Two distinct subgroups of Group B Sox genes for transcriptional activators and repressors: their expression during embryonic organogenesis of the chicken. *Mech Dev* 84: 103–120
- Vaahntomeri K, Karaman S, Mäkinen T, Alitalo K (2017) Lymphangiogenesis guidance by paracrine and pericellular factors. *Genes Dev* 31: 1615–1634
- Wang Y, Nakayama M, Pitulescu ME, Schmidt TS, Bochenek ML, Sakakibara A, Adams S, Davy A, Deutsch U, Luthi U et al (2010) Ephrin-B2 controls VEGF-induced angiogenesis and lymphangiogenesis. *Nature* 465: 483–486
- Wegmann F, Petri B, Khandoga AG, Moser C, Khandoga A, Volkery S, Li H, Nasdala I, Brandau O, Fässler R et al (2006) ESAM supports neutrophil extravasation, activation of Rho, and VEGF-induced vascular permeability. *J Exp Med* 203: 1671–1677
- White MA, Kwasnieski JC, Myers CA, Shen SQ, Corbo JC, Cohen BA (2016) A simple grammar defines activating and repressing cis-regulatory elements in photoreceptors. *Cell Rep* 17: 1247–1254
- Wigle JT, Oliver G (1999) Prox1 function is required for the development of the murine lymphatic system. *Cell* 98: 769–778
- Yang H, Wang H, Shivalila Chikdu S, Cheng Albert W, Shi L, Jaenisch R (2013) One-step generation of mice carrying reporter and conditional alleles by CRISPR/Cas-mediated genome engineering. *Cell* 154: 1370–1379
- Yao Y, Yao J, Boström KI (2019) SOX Transcription Factors in Endothelial Differentiation and Endothelial-Mesenchymal Transitions. *Front Cardiovasc Med* 6: 30
- Zhang Y, Liu T, Meyer CA, Eeckhoute J, Johnson DS, Bernstein BE, Nusbaum C, Myers RM, Brown M, Li W et al (2008) Model-based analysis of ChIP-seq (MACS). *Genome Biol* 9: R137
- Zheng GXY, Terry JM, Belgrader P, Ryvkin P, Bent ZW, Wilson R, Ziraldo SB, Wheeler TD, McDermott GP, Zhu J et al (2017) Massively parallel digital transcriptional profiling of single cells. *Nat Commun* 8: 14049



License: This is an open access article under the terms of the [Creative Commons Attribution-NonCommercial-NoDerivs](https://creativecommons.org/licenses/by-nc-nd/4.0/) License, which permits use and distribution in any medium, provided the original work is properly cited, the use is non-commercial and no modifications or adaptations are made.